© 2020. Published by The Company of Biologists Ltd | Journal of Cell Science (2020) 133, jcs241141. doi:10.1242/jcs.241141

RESEARCH ARTICLE

En bloc TGN recruitment of *Aspergillus* TRAPPII reveals TRAPP maturation as unlikely to drive RAB1-to-RAB11 transition

Mario Pinar and Miguel A. Peñalva*

ABSTRACT

Transport protein particle (TRAPP) complexes regulate membrane traffic. TRAPPII and TRAPPIII share a core hetero-heptamer, also denoted TRAPPI. In fungi TRAPPIII and TRAPPII mediate GDP exchange on RAB1 and RAB11, respectively, regulating traffic across the Golgi, with TRAPPIII also activating RAB1 in autophagosomes. Our finding that *Aspergillus nidulans* TRAPPII can be assembled by addition of a TRAPPII-specific subcomplex onto core TRAPP prompted us to investigate the possibility that TRAPPI and/or TRAPPIII already residing in the Golgi matures into TRAPPII to determine a RAB1-to-RAB11 conversion as Golgi cisternae progress from early Golgi to TGN identity. By time-resolved microscopy, we determine that the TRAPPII reporter Trs120 (the homolog of metazoan TRAPPC9) is recruited to existing trans-Golgi network (TGN) cisternae slightly before RAB11 arrives, and resides for ∼45 s on them before cisternae tear off into RAB11 secretory carriers. Notably, the core TRAPP reporter Bet3 (the homolog of metazoan TRAPPC3) was not detectable in early Golgi cisternae, being instead recruited to TGN cisternae simultaneously with Trs120, indicating *en bloc* recruitment of TRAPPII to the Golgi and arguing strongly against the TRAPP maturation model.

KEY WORDS: GEF, Golgi, RAB GTPase, Exocytosis, Multisubunit tethering complex

INTRODUCTION

Transport protein particle (TRAPP) complexes regulate membrane traffic, acting as guanine nucleotide exchange factors (GEFs) on the RAB GTPases RAB1 and RAB11 (Jones et al., 2000; Morozova et al., 2006; Cai et al., 2008; Pinar et al., 2015; Thomas and Fromme, 2016; Riedel et al., 2017; Thomas et al., 2018, 2019; Pinar et al., 2019). The activation of RAB1 and RAB11 has been intensively studied in *Aspergillus nidulans* and *Saccharomyces cerevisiae*. In these fungi, TRAPP complexes share a 'core hetero-heptamer', also denoted TRAPPI (Fig. 1A), consisting of two copies of Bet3 and one copy each of Trs33, Bet5, Trs23, Trs31 and Trs20 (Fig. 1B, shows equivalences between fungal and metazoan subunit nomenclature), whereas TRAPPII contains the core hetero-heptamer plus Trs120, Trs130, Trs65 and Tca17. In contrast, TRAPPIII differs in the two model organisms, as *A. nidulans* TRAPPIII contains, in addition to the core hetero-heptamer, Trs85 and Tca17, which are also present in *S. cerevisiae* TRAPPIII, and homologs of metazoan TRAPPC11, TRAPPC12 and TRAPPC13, which are absent in budding yeast (Pinar et al., 2019). The actual existence of TRAPPI as an independent entity has been questioned, as this core hetero-heptamer does not exist, as such, in metazoans (Sacher et al., 2018), and appears to be either absent (Thomas et al., 2018) or present in a very minor amount (Pinar et al., 2019) in fungi. Indeed work in yeast led to the conclusion that TRAPPIII, rather than TRAPPI is the TRAPP physiologically activating RAB1 in the secretory pathway of fungi (Thomas et al., 2018). In spite of this fact, we will use in some cases the expression TRAPPI/TRAPPIII (rather than just TRAPPIII) to facilitate reference to previous literature and to acknowledge the unlikely possibility that TRAPPI has a physiological role. In *A. nidulans* TRAPPII is the predominant TRAPP, and is twice as abundant as TRAPPIII (Pinar et al., 2019).

The long (>100 µm) hyphal tip cells of *A. nidulans* are ideally suited for cell biological studies involving 3D (x, y, time) and 4D (x, y, z, time) live microscopy (Peñalva et al., 2012). *A. nidulans* early and late – here denoted *trans*-Golgi network (TGN) – cisternae are resolvable by optical microscopy (Pantazopoulou and Peñalva, 2011), which has been exploited to study the maturation of TGN cisternae into secretory vesicles (SVs). These SVs are transported by actin- and microtubule-dependent motors to the apex (Pantazopoulou et al., 2014; Peñalva et al., 2017), where they form the so-denoted Spitzenkörper (SPK), a fungal-specific accumulation of SVs that await fusion with the plasma membrane (Pantazopoulou et al., 2014; Takeshita et al., 2017; Hernández-González et al., 2018a).

The biogenesis of SVs from TGN cisternae is crucially regulated by RAB11 (Pantazopoulou et al., 2014). In both *A. nidulans* and *S. cerevisiae*, the activation of RAB11 at the TGN is mediated by TRAPPII (Morozova et al., 2006; Pinar et al., 2015, 2019; Riedel et al., 2017; Thomas et al., 2019), thereby reducing the problem of mechanistically understanding the transition between TGN and SV identity to determining how TRAPPII is assembled on, or recruited *de novo* to, TGN cisternae.

In recent work, we established that certain mutations destabilizing TRAPPII result in the formation of two stable subcomplexes, one consisting of the core hetero-hexamer (i.e. TRAPPI) and the second, denoted the TRAPPII-specific subcomplex, consisting of Trs120, Trs130, Trs65 and Tca17 (Pinar et al., 2019). This raised the possibility that TRAPPII is actually assembled by addition of the whole TRAPPII-specific subcomplex onto TRAPP core hetero-heptamers already residing in the Golgi. This possibility was very attractive, given that changes in the composition of TRAPPs shift their substrate specificity from RAB1, activated by TRAPPI/TRAPPIII, to RAB11, activated by TRAPPII (Morozova et al., 2006; Pinar et al., 2015, 2019; Riedel et al., 2017; Thomas et al., 2018, 2019). Thus, TRAPP maturation could drive the transition of RAB1 into RAB11, thereby governing traffic across the Golgi by programmed RAB conversion (Morozova et al., 2006; Rivera-Molina and Novick, 2009).

Using fluorescence microscopy, we determine that TRAPPIII is present in exocytic membranous compartments in addition to

Department of Cellular and Molecular Biology, Centro de Investigaciones Biológicas CSIC, Ramiro de Maeztu 9, 28040 Madrid, Spain.

*Author for correspondence (penalva@cib.csic.es)

M.A.P., 0000-0002-3102-2806

Handling Editor: David Stephens
Received 4 November 2019; Accepted 6 April 2020

Journal of Cell Science (2020) 133, jcs241141. doi:10.1242/jcs.241141

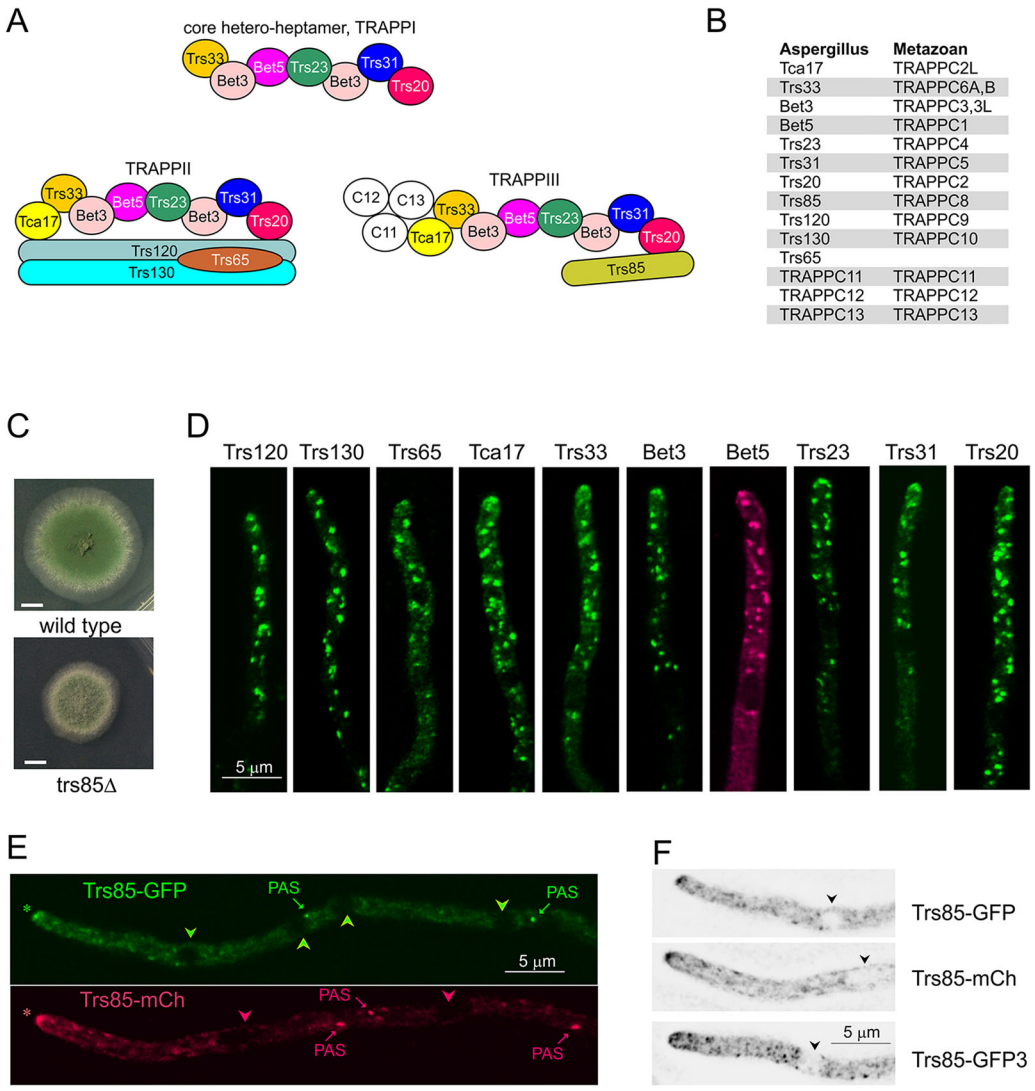

Fig. 1. Subcellular localization of TRAPPs. (A) Schemes depicting the subunit composition of *A. nidulans* TRAPPs (Pinar et al., 2019). (B) Nomenclature of TRAPP subunits. (C) *trs85*Δ weakly impairs growth. The two colonies are shown at the same magnification (as indicated by the reference bar). (D) Localization of core TRAPP and TRAPPII subunits to punctate structures resembling TGN cisternae. All proteins were tagged endogenously with GFP or GFPx3 excepting Bet5, which was tagged with mCherry. (E) Localization of Trs85 (TRAPPIII) tagged with different fluorescent tags. The presence of Trs85 in the SPKs is indicated with asterisks. 'Empty' nuclei and PASs are indicated with arrowheads and arrows, respectively. (F) Trs85–GFPx3 allows better definition of small puncta standing out against the cytosolic haze. Nuclei are indicated with arrowheads. PASs are not visible because they usually form further away from the tip. All fluorescence microscopy images are maximal intensity projections of Huygens-deconvolved *Z*-stacks.

localizing to pre-autophagosomal structures (PASs), and study the consecutive arrival of TRAPPII and RAB11 to extant TGN cisternae. Using 3D and 4D microscopy, we determined that Bet3 strictly colocalizes with TRAPPII on TGN cisternae over time, rebutting a model in which the conversion of TRAPPI/TRAPPIII into TRAPPII governs the maturation of RAB1 into RAB11 and thus traffic across and exit from the Golgi.

RESULTS

Revisiting the localization of the TRAPPIII component Trs85

In fungi, RAB1 plays roles in autophagy (Lynch-Day et al., 2010; Pinar et al., 2013b), in addition to exocytic roles in the ER/Golgi interface (Lord et al., 2011) and the TGN (McDonold and Fromme, 2014). It was widely accepted that TRAPPIII would only regulate the autophagic functions of RAB1, whereas TRAPPI would regulate the Golgi functions. However, a recent report concluded that *S. cerevisiae* TRAPPI does not exist as such, and that it is actually TRAPPIII that regulates all functions of RAB1, including those in the ER/Golgi interface and in the TGN (Thomas et al., 2018). This conclusion was buttressed by recent data strongly indicating that TRAPPI is present in very minor amounts, if at all, in *A. nidulans* (Pinar et al., 2019). However, the role of TRAPPIII required further investigation because partial localization of Trs85 to Sec7-containing Golgi cisternae in non-autophagic yeast cells (Thomas et al., 2018) is consistent with the TGN role but inconsistent with the ER/Golgi role.

A. nidulans growth is exquisitely sensitive to secretory pathway impairment. *trs85*Δ causes a colony growth defect (Fig. 1C) that is difficult to reconcile with an strictly autophagic role of TRAPPIII [*atg*Δ mutations do not affect growth (Pinar et al., 2013b)]. Thus, we revisited the localization of Trs85, comparing it with that of every other TRAPP component, endogenously tagged with fluorescent proteins. With the exception of Trs33 and Trs65, all these other proteins are essential. Therefore, that the corresponding strains are

Journal of Cell Science (2020) 133, jcs241141. doi:10.1242/jcs.241141

viable indicates that tagging does not preclude function. Trs85–GFP is also functional, as judged by its ability to restore the growth defect resulting from *trs85*Δ (Fig. S1).

Trs120–GFP localizes to TGN cisternae (Pinar et al., 2015) (see below). Fig. 1D shows that all GFP-tagged core TRAPP and TRAPPII reporters localize similarly to Trs120–GFP, that is they localize to TGN-like cisternae, strongly polarized towards the tip, with faint staining of the SPK. [For Bet5, we used Bet5–mCherry (mCh), as Bet5–GFP was largely cytosolic.] Using similar image acquisition conditions, Trs85–GFP clearly accumulated on pre-autophagosomes (PASs), circumscribed to regions located far away from the tips (Fig. 1E) (Pinar et al., 2013b). In addition, Trs85–GFP was weakly localized to the SPK, as well as to a cytosolic 'haze' against which numerous faint small puncta were barely noticeable and 'empty' nuclei appeared as 'fluorescence-free' ovals (Fig. 1E, arrowheads). Increased exposure times combined with image deconvolution served to confirm the presence of Trs85–GFP fluorescence at the SPK and made the presence of the small puncta, clearly predominating ahead of the apicalmost nucleus, more apparent against the cytosolic haze (Fig. 1F). The definition of these puncta was further improved after endogenously tagging Trs85 with tandemly triplicated GFP (GFPx3) (Fig. 1F) (the growth test shown in Fig. S1 shows that Trs85–GFPx3 is also functional). These TRAPPIII (Trs85) puncta are clearly distinct from TGN cisternae in that they are markedly smaller and far more numerous than the latter (compare cells in Fig. 1D and E,F displayed at the same magnification). That Trs85–mCh localized like Trs85–GFP (Fig. 1E) argues against the possibility that the observed Trs85 localization was a tagging artifact.

The faint fluorescence of the small Trs85 puncta, as well as the strong cytosolic haze, precluded *in vivo* colocalization studies. However, the presence of Trs85 at the SPK (an accumulation of secretory vesicles) points to a role for TRAPPIII in the exocytic pathway, and it is tempting to speculate that the faint, polarized punctate structures containing Trs85, that are different in size and abundance from TGN cisternae, reflect the activation of RAB1 by TRAPPIII at early Golgi compartments (see also Discussion).

The TRAPPII component Trs120 cycles on TGN cisternae

A previous study with *S. cerevisiae* concluded that Trs31 (a core TRAPP) colocalized with TRAPPII, but not with an early Golgi marker, suggesting that TRAPP complex(es) other than the TGN-located TRAPPII were difficult to visualize by fluorescence microscopy (Montpetit and Conibear, 2009). In contrast, another study concluded that Bet3 (also a core TRAPP), although colocalizing with TRAPPII, did so incompletely (Thomas et al., 2018). Because Golgi maturation processes might affect the localization of TRAPP complexes over time, for example, if TRAPPI/TRAPPIII itself 'matures' into TRAPPII, we decided to investigate the colocalization of a core TRAPP subunit with the TRAPPII-specific Trs120 reporter by time-resolved microscopy, aiming to detect a class of cisternae containing the former but not the latter. To improve the time resolution (*Tr*) of previous studies (Pinar et al., 2015), we tagged Trs120 endogenously with GFPx3. Trs120–GFPx3 is markedly brighter than Trs120–GFP, supports vigorous growth and requires lower exposure time, improving *Tr* and allowing for longer periods of imaging without cell photodamaging. Trs120–GFPx3 localizes to polarized TGN cisternae (Fig. 2A), whose average lifetime is 2 min (Pantazopoulou et al., 2014). Trs120 is recruited at these cisternae only after they are formed and stays until the end of their cycle, when they dissipate into post-Golgi carriers (Pinar et al., 2015). Consequently, cisternae visualized with the 'structural' TGN marker Sec7–tdTomato (tdT) are more abundant than those detected with Trs120–GFPx3 (a proportion of Sec7–tdT cisternae has not yet acquired Trs120) (Fig. 2B), which results in partial colocalization (Fig. 2C) (Pearson's coefficient 0.61±0.05, mean± s.d., n=19 cells).

The kymograph shown in Fig. 2D, derived from Movie 1 consisting of 210 middle planes of a hypha acquired with a *Tr* of 2 fps, illustrates how Trs120–GFPx3 is recruited to TGN cisternae and resides on them until they 'tear off' into post-Golgi carriers bound for the apex. These cycles of recruitment/departure are reflected by slightly tilted, vertical lines whose lengths correspond to the lifetime of Trs120 (TRAPPII) on cisternae. The also tilted line drawn by the growing apex shows that the hypha continues growing (at 0.9 µm min^{-1}) during imaging, demonstrating that these are bona fide *in vivo* observations. Similar kymographs of 3D time series were obtained with Trs120–tdTomato (Fig. S2), Tca17–GFPx3 and Trs130–GFP (Fig. S3A,B, left), showing that fluorescent reporters reflect the behavior of TRAPPII.

To discard the possibility that the recurrence of Trs120–GFPx3 captured by kymographs represented cisterna going in-and-out of focus, we acquired 4D (x, y, z, t) movies, such that each frame was the MIP projection of a Z-stack (Movie 2 shows a hypha growing at 0.63 µm s^{-1}). Kymographs captured a pattern closely resembling that seen with middle planes (Fig. 2F), which was similarly seen using another TRAPPII-specific reporter, Trs130–GFP (Fig. S3B, right) (with 4D time-series a smaller *Tr* results in shorter vertical lines). Thus, the recurrence pattern of fluorescent reporters does not result from cisternae moving out of focus and rather reflects the transient residence of TRAPPII at TGN puncta. Reassured by these results, we analyzed n=78 maturing TGN cisternae extracted from movies acquired with a *Tr* of 1 fps from eight different Trs120–GFPx3 cells, and determined that the time of residence of TRAPPII in TGN cisternae was 44±9 s (mean±s.d.) (Fig. 2E).

Trs120 precedes RAB11 in arrival to TGN cisternae

The above TRAPPII time-of-residence is approximately one-third of the ∼2 min lifetime of a TGN cisterna (Pantazopoulou et al., 2014). As Trs120 (TRAPPII) mediates nucleotide exchange on RAB11, the latter should be recruited to cisternae in parallel to, or after Trs120 accumulates. RAB11 and Trs120 roughly coincide (at low *Tr* of 0.33 fps) in their arrival to the TGN, at the end of the cisternal cycle, before cisternae acquire post-Golgi identity and depart towards the SPK (Pinar et al., 2015). To increase *Tr* we developed a bright mCherry–RAB11 reporter that we combined with Trs120–GFPx3 to acquire 4D movies, recording the red and green channels simultaneously with a beam splitter every 1.2 s (i.e. with a *Tr* of 0.83 fps). Notwithstanding that RAB11 strongly accumulates in the SPK, the two markers colocalized substantially on TGN cisternae (Fig. 3A; Movie 3). Indeed kymographs (Fig. 3B) clearly illustrated the similar patterns of arrival and departure of Trs120 and RAB11, and confirmed that Trs120 substantially colocalizes with RAB11 over time. The strong apical RAB11 signal hindered systematic analysis, but visual examination of the life cycles of n=43 TGN cisternae showed that in 70% the arrival of Trs120 slightly preceded that of RAB11 (Fig. 3B shows an example). That Trs120 slightly precedes RAB11 was confirmed by exploiting the higher *Tr* (2.2 fps) of 3D movies made with middle planes (Fig. 3C).

Core TRAPP subunits also cycle on Golgi cisternae

For co-imaging with Trs120–GFPx3, we chose Bet3 as it contributes two subunits to the complex, which showed to be the

Journal of Cell Science (2020) 133, jcs241141. doi:10.1242/jcs.241141

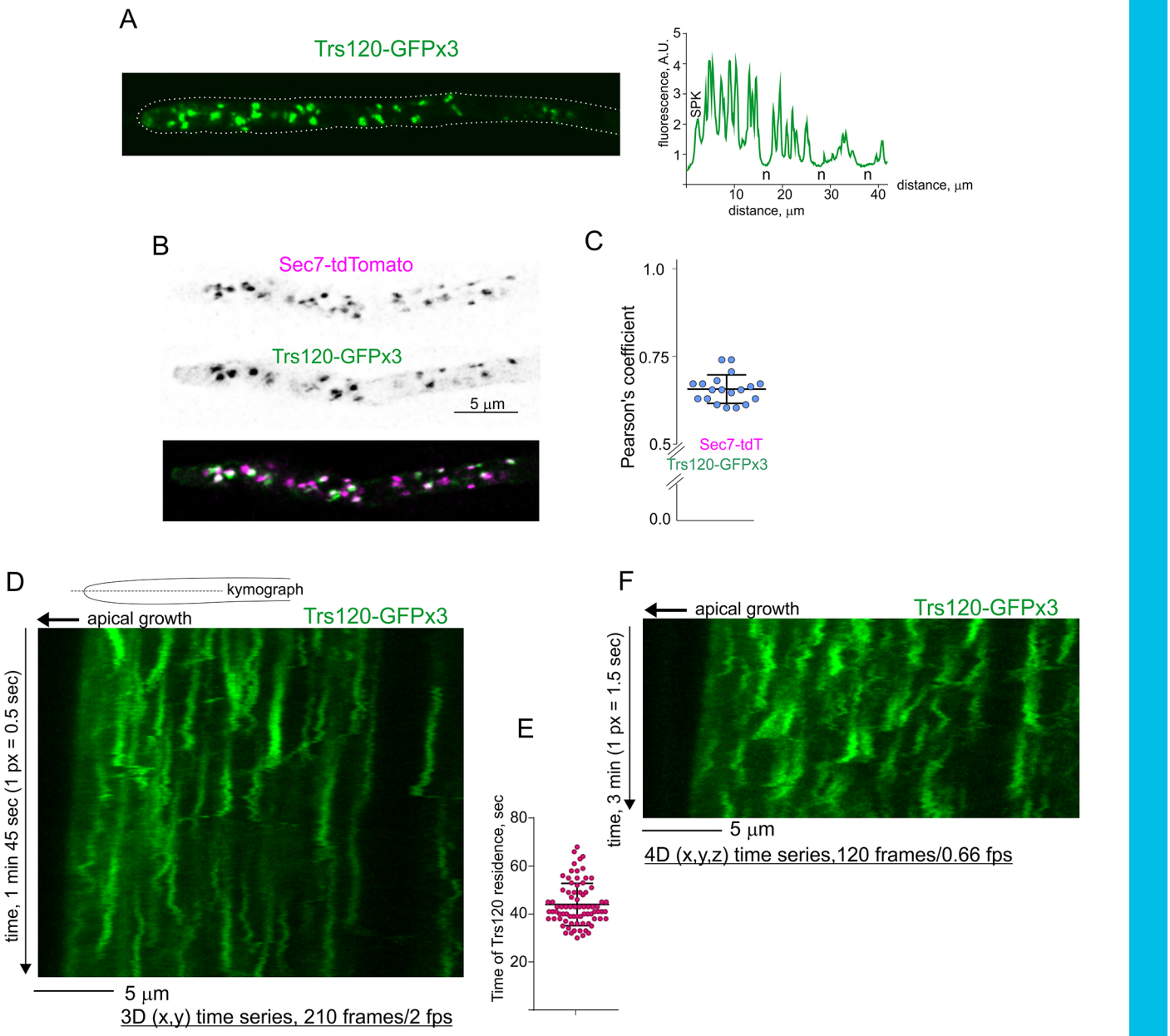

Fig. 2. Transient recruitment of TRAPPII to the TGN. (A) Localization of Trs120–GFPx3 to polarized TGN cisternae. The positions of nuclei (n) are indicated in the linescan. A.U., arbitrary units. (B) Colocalization of Trs120–GFPx3 with Sec7, endogenously tagged with Sec7–tdTomato using simultaneously acquired channels. Images are maximum intensity projections of deconvolved *Z*-stacks. (C) Pearson's coefficient analysis of Trs120 and Sec7 colocalization (*n*=19 cells). (D) Kymograph derived from a Trs120–GFPx3 3D movie acquired with indicated parameters. (E) Time of residence of Trs120–GFPx3 on 78 maturing TGN cisternae obtained from *n*=8 cells. (F) Kymograph derived from a Trs120–GFPx3 4D movie acquired with indicated parameters. Error bars on graphs represent mean±s.d.

brightest among our panel of fluorescent protein-tagged core proteins. Bet3 localized to Golgi-like puncta irrespective of whether it was tagged with GFP, tdT or mCherry, indicating that this represents its physiological localization (Fig. 4A; Fig. S4). Bet3–tdT, consistently most resistant to photodamage, was chosen for colocalization studies. 4D microscopy revealed transient Bet3–tdT localization to cisternae (Movie 4), as seen with Trs120 and Trs130. Fig. 4B shows a kymograph of a Bet3–tdT 2 min sequence with a *Tr* of 1 fps. As with Trs120, the Bet3-containing SPK is seen as a continuous, tilted line reflecting apical extension growth, whereas the transient recruitment of Bet3 to cisternae is reflected in characteristic slightly tilted, vertical lines. This pattern in which the pool of a TRAPP core component builds up in Golgi cisternae before eventually dissipating was confirmed with Trs23–GFPx3 (Fig. S3C).

Bet3 and Trs120 colocalize continuously, disproving the TRAPP conversion model

Next we tried to detect a Golgi compartment containing the TRAPP core but not TRAPPII. In the prevailing model, TRAPPI/TRAPPIII activates RAB1 in the early Golgi whereas TRAPPII activates RAB11 in the TGN (Morozova et al., 2006; Thomas et al., 2019). According to this model, Bet3, which is required for activating both RAB1 and RAB11, should be distributed between early Golgi and TGN cisternae, which are optically resolvable (Pantazopoulou and Peñalva, 2011; Arst et al., 2014; Hernández-González et al., 2014).

Journal of Cell Science (2020) 133, jcs241141. doi:10.1242/jcs.241141

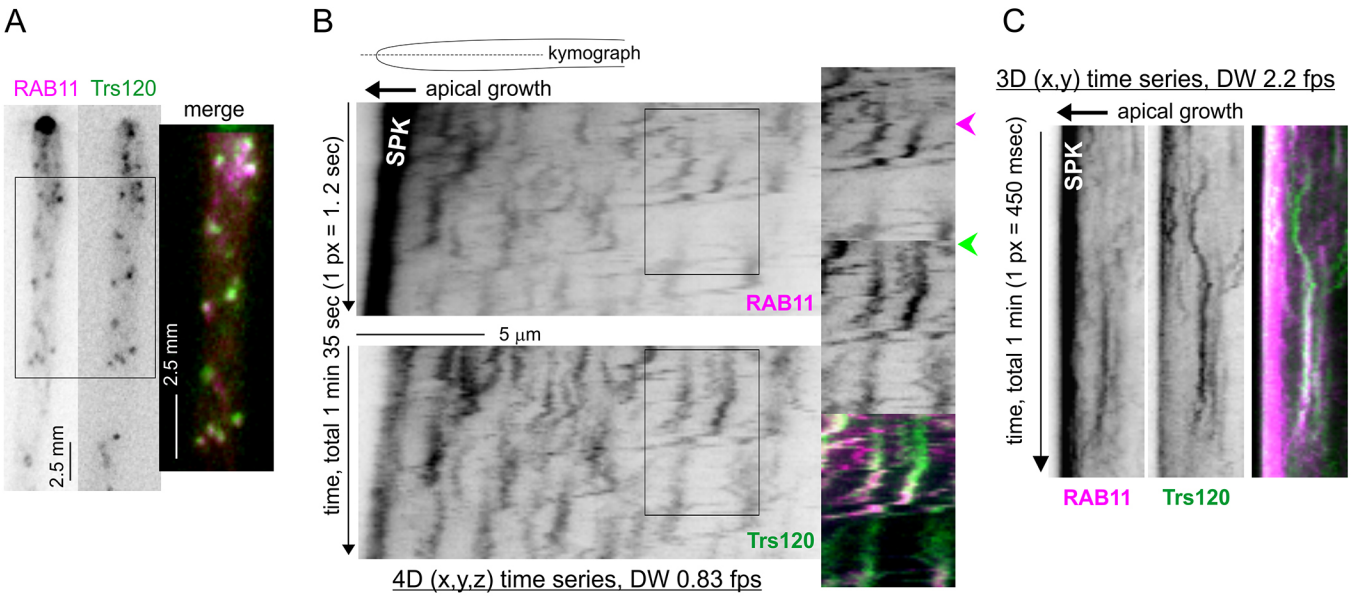

Fig. 3. TRAPPII slightly precedes RAB11 in their arrival to TGN cisternae. (A) Colocalization of mCh–RAB11 and Trs120–GFPx3. Note the strong signal of RAB11 accumulating at the SPK. The two channels were acquired simultaneously. Images are maximum intensity projections of deconvolved *Z*-stacks. (B) Inverted greyscale kymographs for mCh–RAB11 and Trs120–GFPx3, derived from a 4D movie in which the two channels were simultaneously acquired with beam splitter (indicated by DW), using the indicated parameters. The insets including the merge of the two channels show an example of Trs120 accumulating at a TGN cisterna before RAB11 does. Arrowheads indicate the arrival of RAB11 (magenta) and Trs120 (green) to the cisterna. Note that mCh–RAB11 strongly accumulates in the SPK. (C) Example of Trs120–GFPx3 clearly preceding mCh–RAB11 at the cisterna. The kymograph was derived from a 3D movie of middle planes acquired at 2.2 fps with a beam splitter and a 2×2 binning.

Fig. 4C shows that Bet3–tdT and Trs120–GFPx3 completely colocalized (Pearson's coefficient 0.897±0.045, mean±s.d.; Fig. 4D), strongly indicating that a vast majority of core TRAPP is present in cisternae that contain TRAPPII (i.e. TGN cisternae). This result was confirmed after examining visually 667 Bet3–tdT Golgi cisternae (38 hyphae, two independent experiments); 666 contained Trs120, indicating that subclasses of cisternae containing TRAPPI/TRAPPIII only or TRAPPII only do not exist or are below detection by wide-field epifluorescence microscopy. Thus, Bet3 solely localizes to Trs120-containing TGN cisternae. Indeed Bet3–tdT did not colocalize with early Golgi cisternae marked with the GFP-tagged syntaxin Sed5 (Fig. 4C) (Pearson's coefficient 0.138±0.06, mean±s.d., Fig. 4D), whereas it did colocalize with Sec7–GFP to an extent similar to Trs120–tdT (Fig. 4C) (Pearson's of 0.448±0.02 and 0.532±0.061, mean±s.d., respectively; Fig. 4D). (As noted above, incomplete colocalization of Bet3 and Trs120 with the Sec7 TGN marker is attributable to the narrow window-of-residence of TRAPP subunits on TGN cisternae.) Taken together, these experiments argue against distinct TRAPP complexes acting at the transition of early Golgi to TGN cisternae. However, they do not completely rule out the possibility that Bet3 and Trs120 coincide on the same cisternae only transiently, during the period of time in which a hypothetical 'maturation' of TRAPPI/TRAPPIII into TRAPPII would take place in parallel to cisternal maturation. This might occur, for example, if TRAPPII were assembled onto a pre-existing Golgi-localized core TRAPP by addition of TRAPPII-specific subunits (Morozova et al., 2006). To address this possibility, we acquired time-series of Bet3–tdT and Trs120–GFPx3. Fig. 5, Fig. S5A,B and Movie 5 show that the two reporters completely colocalized over time in 3D sequences having a *Tr* of 1–1.4 fps. Moreover, 4D series at 1 fps demonstrated that the coincident pattern of temporal residence of Bet3 and Trs120 on Golgi cisternae does not result from fluorescent puncta going in-and-out of focus (Movie 6; Fig. S5C). Thus, either fluorescent Bet3 forms part of different TRAPPI/TRAPPIII and TRAPPII complexes locating to the same TGN cisternae, or Bet3 and Trs120 belong to the same (TRAPPII) complexes. That Bet3 and Trs120 signals colocalize completely and coincide in their relative intensities, shapes and short-range movements strongly supports the latter interpretation, refuting the TRAPP conversion model.

TRAPPII is the predominant TRAPP complex in *Aspergillus*, being twice as abundant as TRAPPIII (Pinar et al., 2019). In budding yeast a substantial amount of TRAPPIII colocalizes with Sec7 and TRAPPII (Thomas et al., 2018). Thus, we explored the possibility that the high levels of TRAPPII present in TGN puncta mask the presence of core TRAPP subunits associated with TRAPPIII co-existing on the same cisterna. To do this, we deleted *trs120*Δ in a strain carrying a constitutively active *RAB11* allele (denoted *RAB11**, encoding RAB11^{D125E}) to rescue viability (Pinar et al., 2019), which results in the complete absence of TRAPPII (Pinar et al., 2019). Bet3–tdT became almost completely dispersed in *trs120*Δ *RAB11** cells, with few faint, small puncta that were hardly noticeable over the resulting cytosolic haze (Fig. 6A). As *RAB11** by itself does not affect the TGN localization of Bet3–tdT (Fig. S6), this delocalization is attributable to *trs120*Δ. The observation that Bet3–tdT-containing TGN cisternae were not at all noticeable in *trs120*Δ cells is important because it strongly suggests that TRAPPII does not mask the hypothetical presence of substantial amounts of TRAPPIII (or TRAPPI) on TGN membranes. Thus, to reinforce this conclusion we performed the same experiment with another core TRAPP reporter, Trs23–GFPx3, which gave essentially the same results (Fig. 6B). Unfortunately, the identity or dynamics of the few faint, small cytosolic puncta containing TRAPP core proteins could not be addressed by colocalization studies and time-lapse microscopy, as these structures were almost completely obscured by the cytosolic haze.

Journal of Cell Science (2020) 133, jcs241141. doi:10.1242/jcs.241141

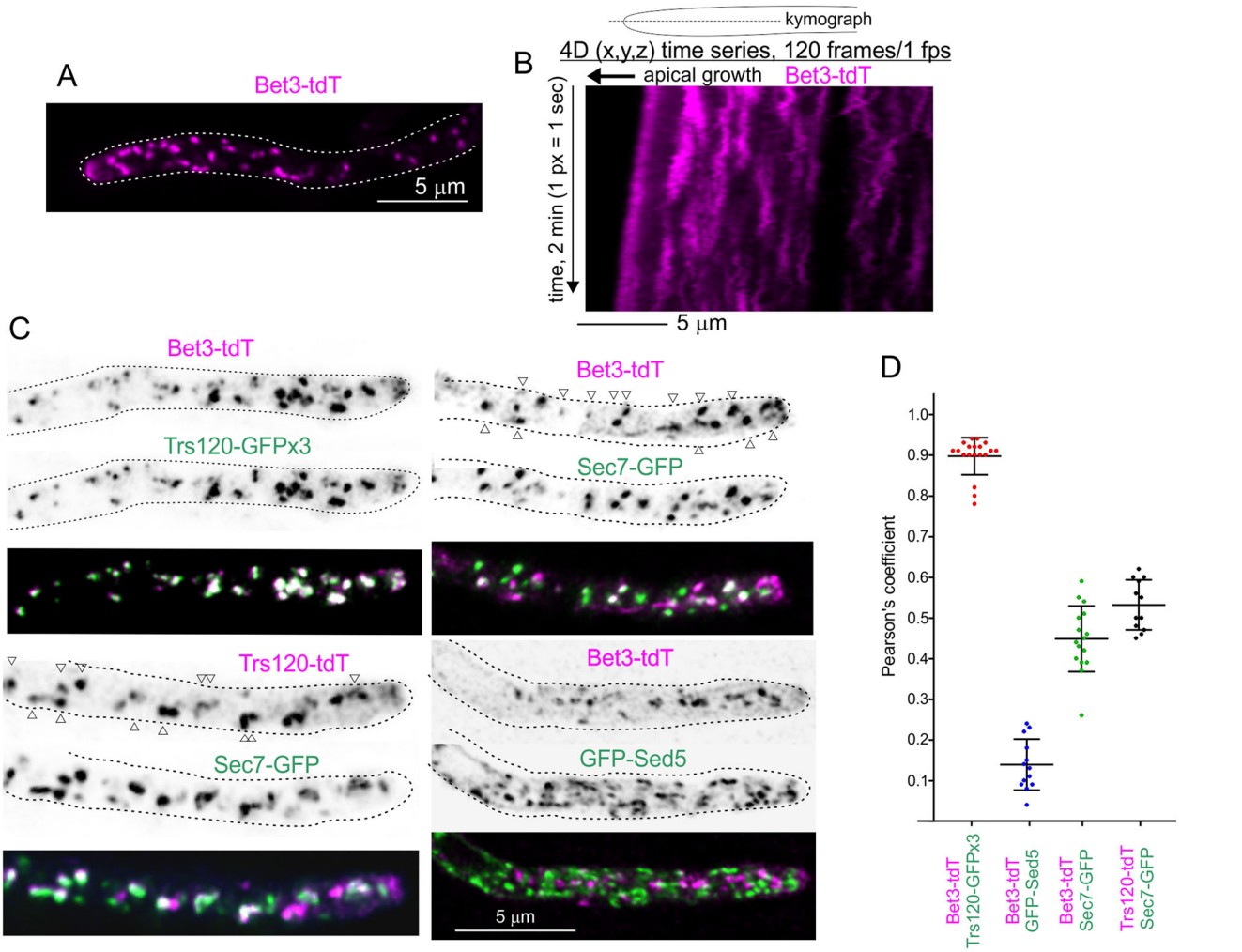

Fig. 4. The core TRAPP component Bet3 transiently localizes to the TGN. (A) Localization of Bet3–tdT to TGN cisternae. (B) Kymograph derived from a 4D movie of Bet3–tdT acquired with the indicated parameters. (C) Colocalization of the indicated pairs of fluorescent proteins. The two channels were acquired simultaneously. Images represent maximum intensity projections of deconvolved *Z*-stacks. Arrowheads highlight colocalizing spots. (D) Pearson's colocalization coefficients for *n*=19 cells expressing Bet3–tdT and Trs120–GFPx3, *n*=13 cells expressing Bet3–tdT and GFP–Sed5, *n*=16 cells expressing Bet3–tdT and Sec7–GFP and *n*=12 cells expressing Trs120–tdT and Sec7–GFP. Error bars on graph represent mean±s.d.

This is visually illustrated by the kymographs in Fig. 6C, which compare the sharp pattern of recurrence of TRAPP on TGN membranes in the wild-type with the hazy pattern of Trs23–GFPx3 in a *trs120*Δ *RAB11** cell (vertical 'empty' sections correspond to nuclei), with hardly any structure noticeable on the hazy background. Of note, as *trs120*Δ markedly increases the levels of TRAPPI at the expense of TRAPPII, but does not affect those of TRAPPIII (Pinar et al., 2019), the cytosolic pattern of core TRAPP markers resulting from TRAPPII ablation would be attributable to the artificial increase in TRAPPI, suggesting that the core TRAPP is not targeted to the Golgi.

We next tested whether TRAPPIII localization was altered by ablating TRAPPII after performing similar experiments with Trs85-GFPx3 in wild-type and *trs120*Δ *RAB11** cells (Fig. 6D). The localization of Trs85/TRAPPIII to a cytosolic haze, the SPK and small punctate structures was essentially undisturbed by *trs120*Δ (Fig. 6D), showing that TRAPPIII localization is TRAPPII-independent.

DISCUSSION

We exploited here the suitability of *A. nidulans* to study intracellular traffic by *in vivo* fluorescence microscopy. In this fungus, intracellular transport involving cooperation between actin- and microtubule-based motors (Abenza et al., 2009, 2010; Zhang et al., 2011, 2014; Taheri-Talesh et al., 2012; Peñalva et al., 2017) resembles that of metazoan cells to a greater extent than that in *S. cerevisiae*. *A. nidulans* hyphal tip cells are particularly useful to investigate the secretory pathway because impairment of exocytosis results in morphological defects (Pinar et al., 2013a,b; Hernández-González et al., 2014), which can facilitate, for example, assessment of whether endogenous tagging of TRAPP subunits with fluorescent proteins negatively affects their function. The Golgi, consisting of scattered early and TGN cisternae, is polarized towards the growing tip (Pantazopoulou and Peñalva, 2009, 2011; Pantazopoulou et al., 2014; Hernández-González et al., 2019), reflecting that exocytosis is targeted to the apex to maintain the supply of cell wall-modifying enzymes and lipids required for rapid growth by apical extension (~1 µm/min at 28°C on microscopy wells) (Hernández-González et al., 2018a). The organization of the Golgi facilitates the analysis, which can be undertaken using kymographs such as those extensively used here, of the fate of large numbers of cisternae over time, which has been exploited to document the maturation of TGN cisternae into post-Golgi RAB11

Journal of Cell Science (2020) 133, jcs241141. doi:10.1242/jcs.241141

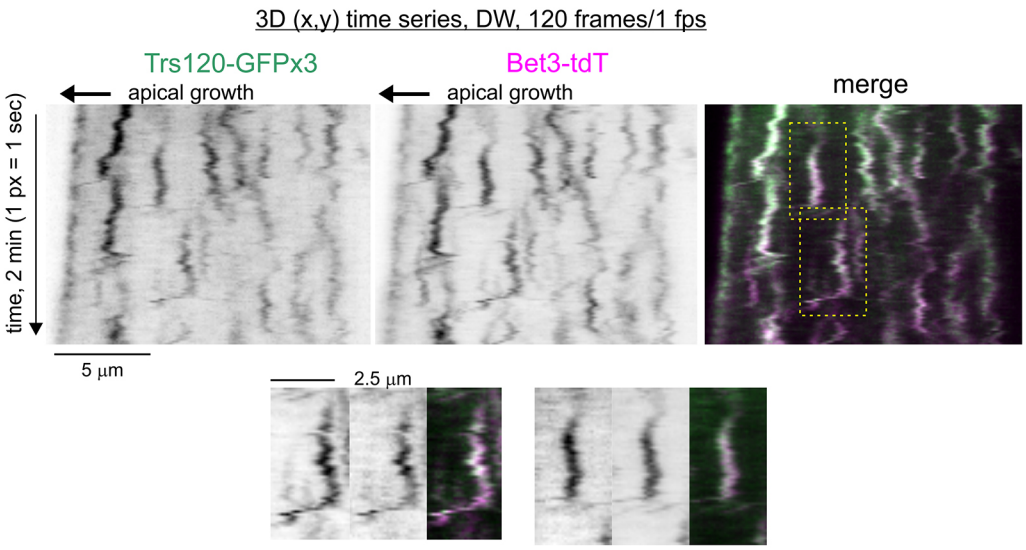

Fig. 5. The core TRAPP component Bet3 and the TRAPPII-specific component Trs120 strictly colocalize on TGN cisternae over time. Kymographs for Trs120–GFPx3 and Bet3–tdT derived from a 2 min 3D movie in which the two channels were simultaneously acquired (DW) every 1 s with a beam splitter. The lower panels show magnified views of the two areas highlighted illustrating how the lifecycles of the two spatially colocalizing proteins strictly overlap over time.

SVs (Pantazopoulou et al., 2014). All these features were exploited here to carry out a comprehensive analysis of TRAPP complexes.

TGN cisternae are transient structures that, at the end of their 2 min lifecycle, become RAB11 carriers destined for the plasma membrane (Pantazopoulou et al., 2014). TRAPPII, which arrives slightly before RAB11, is not an integral component of TGN cisternae, accumulating on them only when a certain stage of maturation is reached. This observation explains why Trs120 colocalizes only partially with Sec7, a constituent marker of the TGN (a proportion of Sec7 cisternae are captured at a maturation stage in which they might not have yet accumulated detectable levels of TRAPPII). The accumulation of TRAPPII in the TGN brings about the activation/recruitment of RAB11, which marks the Golgi-to-SVs transition and the engagement of molecular motors for the transport of these SVs to the SPK (Peñalva et al., 2017; Hernández-González et al., 2018a) (Fig. 7).

An important finding of this work was that *A. nidulans* Trs85, the diagnostic subunit of TRAPPIII, is not exclusive to the PASs, being also detectable in other structures, including SVs concentrated at the SPK, revealing an unexpected and unexplored link between TRAPPIII and exocytosis. Of note, BapH, an effector of RAB11 also localizing to the SPK, connects the latter structure with the autophagy pathway (Pinar and Peñalva, 2017). However, the majority of Trs85 localizes to a cytosolic haze specked with small punctate structures, similar to the Trs85 hazy cytosolic background detected in *S. cerevisiae*, which, in the latter, accounts for 80% of TRAPPIII (Thomas et al., 2018). These *Aspergillus* small punctate structures are much fainter, markedly more abundant and clearly distinct from TGN cisternae, suggesting that they correspond to TRAPPIII activating RAB1 in the ER/early Golgi interface, as suggested for *S. cerevisiae* (Thomas et al., 2018). An observation potentially conflicting with the above conclusion is that ablation of Trs85 causes a relatively small growth defect in an organism exquisitely sensitive to even minor impairments of secretion (Fig. 1C). The likely explanation is that the absence of Trs85 does not preclude the activation of RAB1 for its exocytic role. In previous work, we classified TRAPP subunits according to their essential roles in activating RAB1, RAB11 or both using 'constitutive' mutations of the GTPases that bypass the requirement for their GEFs (Pinar et al., 2019). For example, the viability of *trs120*Δ (TRAPPII) mutants could be rescued by expression of constitutively active RAB11 alone, whereas that of a *bet3*Δ (core) mutant necessitated expression of both constitutively active RAB1 and RAB11, in accordance with the role of certain core hetero-heptamer subunits in the activation of both GTPases (Pinar et al., 2019). *trs20*Δ cells, which contain a TRAPPIII complex devoid of Trs20 and Trs85 (Pinar et al., 2019), could be rescued by expression of constitutive RAB11 alone (Pinar et al., 2019), showing that genetically stripping Trs85 (and Trs20) from TRAPPIII does not preclude the ability of this complex to activate RAB1 in the ER/Golgi interface.

TRAPPI does not exist in *S. cerevisiae* (Thomas et al., 2018) and if it exists at all in *Aspergillus* it would be in minor quantities (Pinar et al., 2019), difficult to detect by microscopy, such that its hypothetical presence in low abundance in the Golgi might be obscured by highly abundant TRAPPII. However, we show here that in *trs120*Δ cells lacking TRAPPII, in which a major proportion of TRAPP is artificially shifted to TRAPPI (Pinar et al., 2019), the core components Bet3 and Trs23 are delocalized to a cytosolic haze. This hazy pattern indicates that TRAPPI is unable to localize to Golgi cisternae, contributing to mounting evidence that it is TRAPPIII rather than TRAPPI that mediates RAB1 activation in the Golgi.

We show that a vast majority of *A. nidulans* TRAPP localizing to the Golgi is accounted for by TRAPPII present at the TGN. Previous work uncovered the possibility that TRAPPII is assembled by adding the stable TRAPPII-specific subcomplex containing Trs120, Trs130, Trs65 and Tca17 onto core TRAPP hetero-heptamers (Pinar et al., 2019). This modular TRAPPII assembly would provide mechanistic support for the model by which core TRAPP already localized to the Golgi would mature into TRAPPII as cisternal maturation progresses, determining the transition between RAB1 and RAB11 stages (Morozova et al., 2006). As this core TRAPP is unlikely to proceed from TRAPPI, it would be TRAPPIII which would mature into TRAPPII by substituting TRAPPIII-specific subunits with TRAPPII-specific ones. In this scenario, Trs85 in TRAPPIII would compete with Trs120 in TRAPPII for its Trs20 recruiter to the TRAPP core, and therefore Trs85 would need to be stripped from the core to permit the subsequent assembly of TRAPPII. However, this possibility appears difficult to reconcile with the stable association of Trs85 to the core complex in TRAPPIII (Pinar et al., 2019). Moreover, in *trs120*Δ cells, in which TRAPPII is absent and therefore cannot obscure TRAPPIII detection, TGN cisterna cannot be visualized with core TRAPP reporters (Fig. 6), even though *trs120*Δ does not affect the amount

Journal of Cell Science (2020) 133, jcs241141. doi:10.1242/jcs.241141

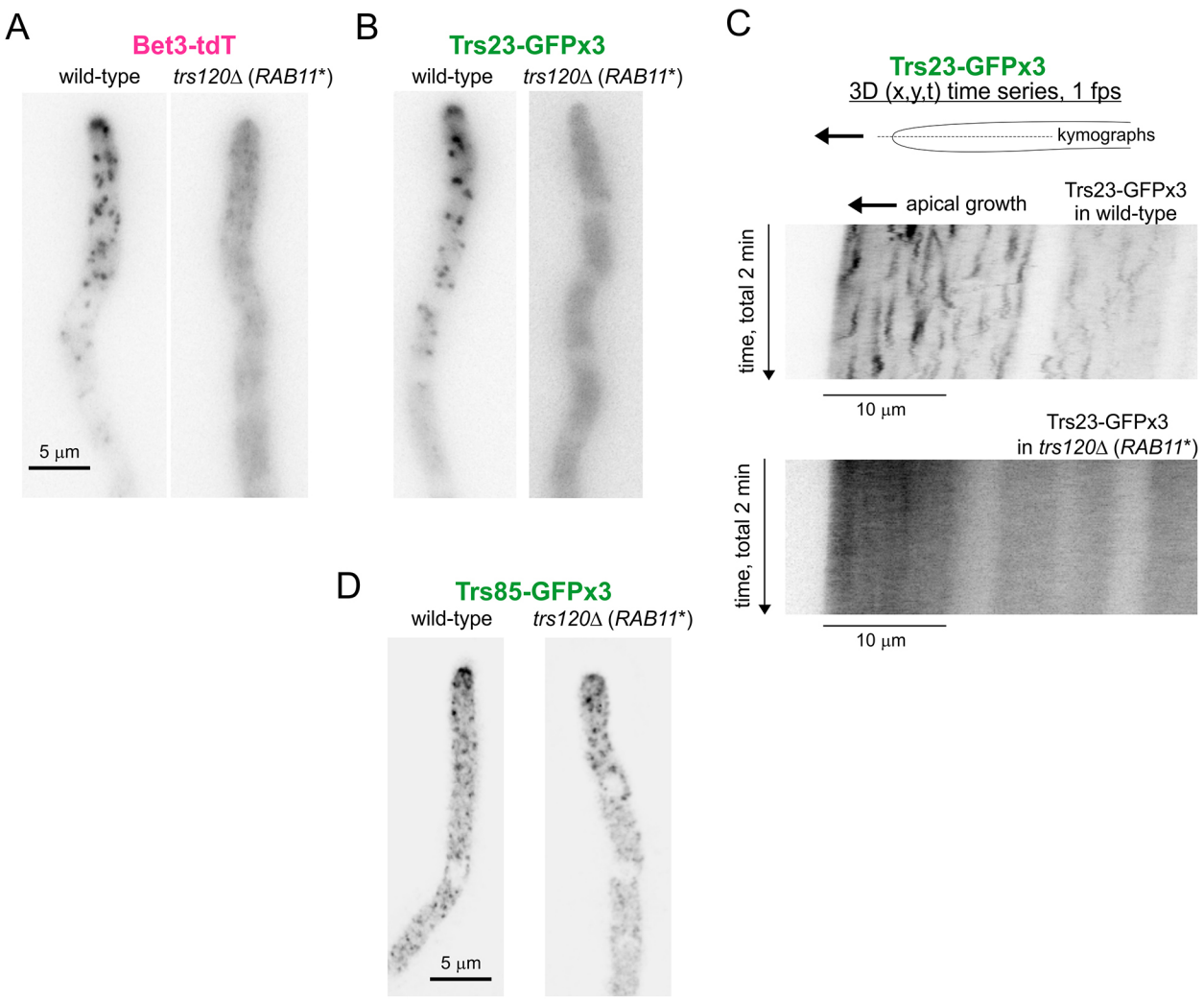

Fig. 6. Localization of core TRAPP components and the TRAPPIII component Trs85 in the absence of TRAPPII. (A) Localization of Bet3–tdT in the wild-type and in *trs120*Δ cells lacking TRAPPII (rescued with *RAB11**). Images are maximum intensity projections (MIPs) of *Z*-stacks that were not deconvolved to preserve the original signal intensities. (B) Localization of Trs23–GFPx3 in the wild-type and in *trs120*Δ cells lacking TRAPPII (rescued with *RAB11**); *Z*-stack-derived images were acquired as in A. (C) Kymographs depicting the localization of Trs23–GFPx3 over time, derived from movies acquired with a *Tr* of 1 fps. (D) Trs85-GFPx3 (TRAPPIII) localization is not affected by ablation of TRAPPII. Images are MIPs of deconvolved *Z*-stacks. All cells are shown at the same magnification.

of TRAPPIII present (Pinar et al., 2019). Finally, *trs120*Δ does not affect the normal localization of Trs85-labeled TRAPPIII to a cytosolic haze and to weakly bright puncta that are clearly smaller than TGN cisternae, suggesting that TRAPPII and TRAPPIII do not compete for the same core TRAPP. This apparent absence of TRAPPIII in the *Aspergillus* TGN contrasts with the situation in *S. cerevisiae*, where a detectable amount of TRAPPIII colocalizes with the TGN reporter Sec7 (Thomas et al., 2018). We note, however, that we cannot rule out the possibility that small, faint Trs85 puncta represent specialized domains of TGN cisternae. Addressing this possibility will require developing brighter fluorescent reporters for Trs85 combined with super-resolution microscopy.

In any case, the maturation model predicts that a proportion of Golgi cisternae should contain TRAPP core subunits but not Trs120. However, still images of core TRAPP and TRAPPII-specific components showed that all localized to TGN-like puncta. Moreover, the Bet3 core TRAPP component showed a similar degree of colocalization with Sec7 to Trs120, arguing against the above possibility. As Trs23 and Bet3 ‘cycle’ on TGN cisternae in a similar manner to what is seen with Trs120, we then considered the possibility that core components peak on TGN cisternae before TRAPPII-specific components do. However, Bet3–tdT and Trs120–GFPx3 completely colocalized over time, both appearing and dissipating simultaneously, which argues against them accumulating at different time points of the cisternal cycle. Instead, the complete colocalization, the coincident shapes of Bet3 and Trs120 kymograph traces, and the correlating brightness of the two reporters strongly indicate that Bet3 and Trs120 belong to the same TRAPPII complexes, negating the ‘TRAPP maturation’ model.

A key implication of these findings is that TRAPPII is recruited as a whole to extant TGN cisternae. The TGN mediates endocytic recycling both in yeast (Day et al., 2018) and in *A. nidulans* (Hernández-González et al., 2018a), but efficient endocytic recycling in the latter fuels hyphal growth, which might have resulted in species-specific features in the regulation of the TGN. It is plausible that TRAPPII monitors, and responds to, the arrival at TGN cisternae of membranous carriers of endocytic origin that

Journal of Cell Science (2020) 133, jcs241141. doi:10.1242/jcs.241141

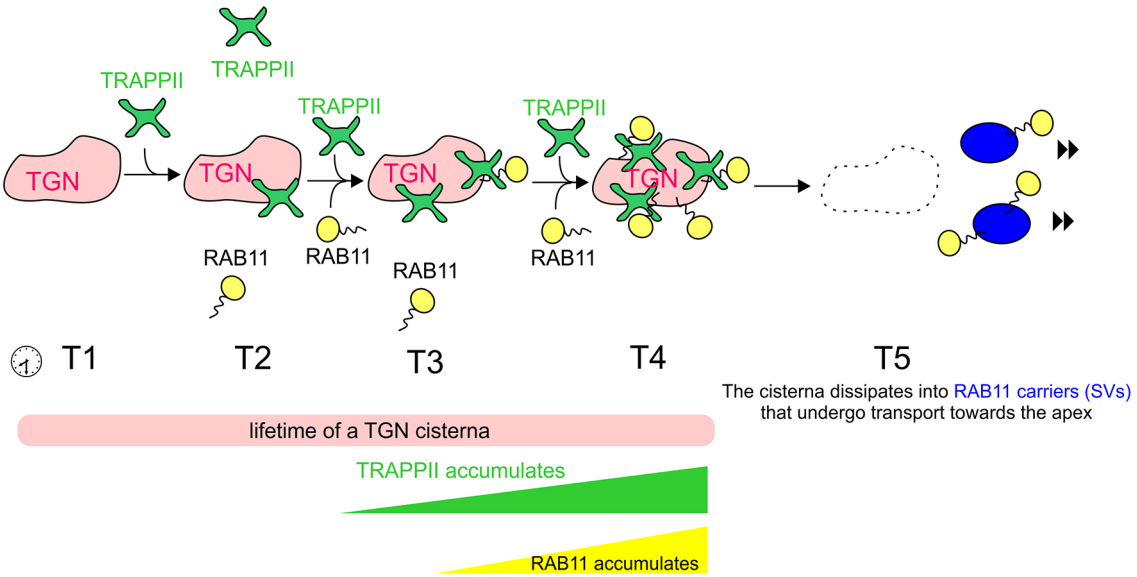

Fig. 7. A model for the biogenesis of SVs from TGN cisternae. TRAPPII is recruited *en bloc* to a TGN cisterna during approximately the second half of its lifecycle, accumulating on it and leading to the recruitment of RAB11. When levels of RAB11 reach a certain threshold the cisterna dissipates into RAB11-containing post-Golgi carriers that are transported by molecular motors to the apex. TRAPPII is depicted with its approximate shape determined by EM (Yip et al., 2010; Pinar et al., 2019) to incorporate the concept that the separation of the TRAPPII active site from the plane of the membrane makes it accessible to RAB11, but not to RAB1 (Thomas et al., 2019). T1-T5 are different times during the maturation of a TGN cisterna.

carry cargo recycling to the PM in a Sec7- and RAB11-dependent manner (Hernández-González et al., 2018a). This would be consistent with the report that Trs120 mediates traffic from early endosomes to the TGN in yeast (Cai et al., 2005). Thomas and Fromme (2016) have shown that both the recruitment of TRAPPII to TGN-like liposomes and its GEF activity on RAB11 are dependent on active ARF1 and anionic glycerophospholipids. Future investigations will focus on the regulation of these processes.

MATERIALS AND METHODS

Aspergillus media, culture conditions and transgenes

Standard *A. nidulans* media were used for strain propagation and conidiospore production (Pinar and Peñalva, 2017; Hernández-González et al., 2018b). Genetic techniques used were as described previously (Todd et al., 2007). Strains are listed in Table S1.

Endogenous gene tagging with fluorescent protein tags

A plasmid containing the *rab11* (also known as *rabE*) promoter upstream of the mCherry–RAB11 coding region, followed by the 3′-UTR of the gene and the *A. fumigatus pyrG* gene, used as selective marker, was integrated in the *rab11* locus as described for its GFP–RAB11 equivalent (Pantazopoulou et al., 2014), such that the resulting strains contained a untagged copy of *rab11* besides the mCherry-tagged one. The correct integration event was confirmed by Southern blotting. All other genes were endogenously tagged with fluorescent proteins using PCR-assembled linear DNA cassettes and homology-driven recombination. Single GFP and mCherry tagging used template plasmids carrying a *(Gly-Ala)5-GFP::pyrG*^{Af} and *(Gly-Ala)5-mCherry::pyrG*^{Af}. Endogenously tagged genes encoding Trs120–GFP, Trs85–GFP and Sec7–GFP had been reported previously (Pantazopoulou and Peñalva, 2009; Pinar et al., 2013b, 2015). Here, we tagged Bet3, Bet5, Trs20, Trs23, Trs31, Trs33, Trs65, Trs130 and Tca17 with a single GFP, and Trs85, Bet3 and Bet5 with mCherry (see Table S1). Trs23, Bet5, Trs120, Trs31, Tca17 and Trs85 were additionally labeled with GFPx3, consisting of three copies of EGFP in tandem each carrying, at the N-terminus, a $(Gly\text{-}Ala)_5$ spacer. DNA encoding this chimera (*A. nidulans* codon usage-adapted) was synthesized by ATG:: biosynthetics (Merzhausen, Germany) and supplied as a 5′-*SbfI-AcsI*-(GFPx3)-*NotI-XmaI*-3′ DNA fragment cloned in pBS-KSII. PCR-amplified DNA fragments, flanked by *SbfI* and AcsI sites and containing gene-specific coding-regions, were fused in frame to the GFPx3 coding region, thus generating an intermediate plasmid into which PCR DNA fragments, flanked by *Not*I and *Xma*I sites at their 5′- and 3′-ends, respectively, and containing gene-specific 3′-flanking regions fused to the *A. fumigatus pyrG* gene, were cloned in the intermediate plasmid after *NotI* and *XmaI* digestion. The complete cassette was excised after digestion with *SbfI* and *XmaI* and used to select pyrimidine independent transformants of MAD5736 or MAD6512, as appropriate, to generate tagged strains carrying compatible pairs of auxotrophic markers for subsequent crossing. An identical strategy was used to C-terminally tag genes encoding Trs120, Bet3 and Sec7 with tandem-dimer Tomato fluorescent protein (tdT), whose coding region was also synthesized with *A. nidulans*-optimized codon usage.

Microscopy

Hyphae imaged by epifluorescence microscopy were cultured in pH 6.8 ‘watch minimal medium’ (WMM) (Peñalva, 2005) at 28°C, using eight-well chambers (IBIDI GmbH, Martinsried, Germany or Lab-Tek, Nalge Nunc International, Rochester, NY). Images were acquired with Leica DMI6000 B inverted microscopes equipped with Leica 63×/1.4 N.A. Plan Apochromatic objectives and driven by Metamorph Premier software (Molecular Dynamics). The temperature of the cultures was controlled with a Heating Insert P on-stage incubator (Leica) combined with an objective heater (PeCon GmbH, Germany), as described previously (Pinar et al., 2013a), or with a Leica incubation hood enclosing the whole microscope. Leica EL6000 light sources provided excitation light. The microscopes were coupled to Hamamatsu ORCA-ER CCD (1344×1024 pixels, 6.45 µm cell size) and Orca-Flash 4.0LT CMOS (2048×2048 pixels; 6.5 µm cell size) cameras. Single-channel acquisition of fluorescence images was made with Semrock GFP-3035B and TXRED-4040B ‘BrightLine’ filter cubes. All colocalization experiments were made with images acquired simultaneously in the two channels with either a Photometrics Dual-View beam splitter (CCD camera) or a Gemini beam splitter (Hamamatsu) equipped with Chroma ET632/60 and Semrock 01-512/25 emission filters (CMOS camera). The dual excitation filter in the microscope was a Chroma 59022-ET for EGFP/mCherry. Precise alignment of Dual View channels was carried out using fluorescent beads (TetraSpeck microspheres, blue/green/orange/dark red; Molecular Probes) as references and the ‘color-align’ menu of Metamorph software. Alignment of the Gemini channels used the software provided by the manufacturer.

3D (x, y, t) and 4D (x, y, z, t) stacks of images were acquired with the minimal settings of the excitation source that provided a sufficient signal, with an appropriate exposure time, to prevent cell photodamage. To improve time resolution in 4D acquisitions, *Z*-stacks of images acquired with a Z-pass of 0.25–0.5 µm were transferred to the computer RAM using the 'stream acquisition' function of Metamorph. Channels were merged using the 'color align' Metamorph plug in. Movies of maximal intensity projections of the *Z*-stacks were constructed with the 'review multidimensional acquisition' plugin of Metamorph. Annotated movies were converted to QuickTime format using ImageJ and file size-adjusted using mpeg-4 compression.

Image manipulation and analysis

All still images shown correspond to *Z*-stacks deconvolved with Huygens Professional for Win64. Images and time series were converted to 8-bit monochrome or 24-bit RGB and annotated with Corel Draw (Corel, Ottawa, Canada). For colocalization analyses using the Pearson's coefficient, *Z*-stacks of images in the GFP and red (tdT or mCherry) channels acquired with a beam splitter were deconvolved with Huygens software. Pearson's coefficients were determined with the Coloc 2 plugin of FIJI (ImageJ 1.52), using the corresponding maximal intensity projections and manually traced regions of interest (ROIs) covering the apex-proximal region of the hyphae containing the greatest abundance of Golgi cisternae and excluding the nuclei. Datasets for each combination of markers were analyzed with Prism 3.02 (GraphPad software). To determine the effects of *trs33*Δ in the recruitment of Trs120–GFP to TGN cisternae, 5 µm-deep *Z*-stacks of wt and *trs33*Δ cells expressing Trs120–GFP were acquired with the same settings. Maximal intensity projections of these images were thresholded to include only the fluorescence signal present in Golgi puncta in the apical-most 20 µm of the hyphae and the total amount of signal within the thresholded area was calculated and plotted with Prism 3.02.

Acknowledgements

We thank Herb Arst for critical reading of the manuscript and Ana Alonso for skillful technical assistance. The genomic and transcriptomic sequence data used to confirm the N- and C-termini of TRAPP subunits were produced by the Genome Projects supported by Genome Canada and Génome Québec (http://www.fungalgenomics.ca) and were made available through Prof. Adrian Tsang of Concordia University.

Competing interests

The authors declare no competing or financial interests.

Author contributions

Conceptualization: M.P., M.A.P.; Methodology: M.P., M.A.P.; Validation: M.P., M.A.P.; Formal analysis: M.P., M.A.P.; Investigation: M.P., M.A.P.; Resources: M.P.; Data curation: M.P.; Writing - original draft: M.A.P.; Writing - review & editing: M.A.P.; Visualization: M.A.P.; Supervision: M.A.P.; Funding acquisition: M.A.P.

Funding

Work supported by Ministerio de Ciencia, Innovación y Universidades (grants BIO2015-65090R and RTI2018-093344-B-I00) and Comunidad de Madrid (grants S2017/BMD-3691, InGEMICS-CM) to M.A.P.

Supplementary information

Supplementary information available online at http://jcs.biologists.org/lookup/doi/10.1242/jcs.241141.supplemental

Peer review history

The peer review history is available online at https://jcs.biologists.org/lookup/doi/10.1242/jcs.241141.reviewer-comments.pdf

References

Abenza, J. F., Pantazopoulou, A., Rodríguez, J. M., Galindo, A. and Peñalva, M. A. (2009). Long-distance movement of *Aspergillus nidulans* early endosomes on microtubule tracks. *Traffic* **10**, 57-75. doi:10.1111/j.1600-0854.2008.00848.x

Abenza, J. F., Galindo, A., Pantazopoulou, A., Gil, C., de los Ríos, V. and Peñalva, M. A. (2010). *Aspergillus* RabB^{Rab5} integrates acquisition of degradative identity with the long-distance movement of early endosomes. *Mol. Biol. Cell* **21**, 2756-2769. doi:10.1091/mbc.e10-02-0119

Arst, H. N., Jr., Hernández-González, M., Peñalva, M. A. and Pantazopoulou, A. (2014). GBF/Gea mutant with a single substitution sustains fungal growth in the absence of BIG/Sec7. *FEBS Lett.* **588**, 4799-4806. doi:10.1016/j.febslet.2014.11.014

Cai, H., Zhang, Y., Pypaert, M., Walker, L. and Ferro-Novick, S. (2005). Mutants in *trs120* disrupt traffic from the early endosome to the late Golgi. *J. Cell Biol.* **171**, 823-833. doi:10.1083/jcb.200505145

Cai, Y., Chin, H. F., Lazarova, D., Menon, S., Fu, C., Cai, H., Sclafani, A., Rodgers, D. W., De La Cruz, E. M., Ferro-Novick, S. et al. (2008). The structural basis for activation of the Rab Ypt1p by the TRAPP membrane-tethering complexes. *Cell* **133**, 1202-1213. doi:10.1016/j.cell.2008.04.049

Day, K. J., Casler, J. C. and Glick, B. S. (2018). Budding yeast has a minimal endomembrane system. *Dev. Cell* **44**, 56-72.e54. doi:10.1016/j.devcel.2017.12.014

Hernández-González, M., Peñalva, M. A. and Pantazopoulou, A. (2014). Conditional inactivation of *Aspergillus nidulans sarA*^{SAR1} uncovers the morphogenetic potential of regulating endoplasmic reticulum (ER) exit. *Mol. Microbiol.* **95**, 491-508. doi:10.1111/mmi.12880

Hernández-González, M., Bravo-Plaza, I., Pinar, M., de los Ríos, V., Arst, H. N., Jr and Peñalva, M. A. (2018a). Endocytic recycling via the TGN underlies the polarized hyphal mode of life. *PLoS Genet.* **14**, e1007291. doi:10.1371/journal.pgen.1007291

Hernández-González, M., Pantazopoulou, A., Spanoudakis, D., Seegers, C. L. C. and Peñalva, M. A. (2018b). Genetic dissection of the secretory route followed by a fungal extracellular glycosyl hydrolase. *Mol. Microbiol.* **109**, 781-800. doi:10.1111/mmi.14073

Hernández-González, M., Bravo-Plaza, I., de Los Ríos, V., Pinar, M., Pantazopoulou, A. and Peñalva, M. A. (2019). COPI localizes to the early Golgi in *Aspergillus nidulans*. *Fungal Genet. Biol.* **123**, 78-86. doi:10.1016/j.fgb.2018.12.003

Jones, S., Newman, C., Liu, F. and Segev, N. (2000). The TRAPP complex is a nucleotide exchanger for Ypt1 and Ypt31/32. *Mol. Biol. Cell* **11**, 4403-4411. doi:10.1091/mbc.11.12.4403

Lord, C., Bhandari, D., Menon, S., Ghassemian, M., Nycz, D., Hay, J., Ghosh, P. and Ferro-Novick, S. (2011). Sequential interactions with Sec23 control the direction of vesicle traffic. *Nature* **473**, 181-186. doi:10.1038/nature09969

Lynch-Day, M. A., Bhandari, D., Menon, S., Huang, J., Cai, H., Bartholomew, C. R., Brumell, J. H., Ferro-Novick, S. and Klionsky, D. J. (2010). Trs85 directs a Ypt1 GEF, TRAPPIII, to the phagophore to promote autophagy. *Proc. Natl. Acad. Sci. USA* **107**, 7811-7816. doi:10.1073/pnas.1000063107

McDonold, C. M. and Fromme, J. C. (2014). Four GTPases differentially regulate the Sec7 Arf-GEF to direct traffic at the trans-golgi network. *Dev. Cell* **30**, 759-767. doi:10.1016/j.devcel.2014.07.016

Montpetit, B. and Conibear, E. (2009). Identification of the Novel TRAPP Associated Protein Tca17. *Traffic* **10**, 713-723. doi:10.1111/j.1600-0854.2009.00895.x

Morozova, N., Liang, Y., Tokarev, A. A., Chen, S. H., Cox, R., Andrejic, J., Lipatova, Z., Sciorra, V. A., Emr, S. D. and Segev, N. (2006). TRAPPII subunits are required for the specificity switch of a Ypt-Rab GEF. *Nat. Cell Biol.* **8**, 1263-1269. doi:10.1038/ncb1489

Pantazopoulou, A. and Peñalva, M. A. (2009). Organization and dynamics of the *Aspergillus nidulans* Golgi during apical extension and mitosis. *Mol. Biol. Cell* **20**, 4335-4347. doi:10.1091/mbc.e09-03-0254

Pantazopoulou, A. and Peñalva, M. A. (2011). Characterization of *Aspergillus nidulans* RabC/Rab6. *Traffic* **12**, 386-406. doi:10.1111/j.1600-0854.2011.01164.x

Pantazopoulou, A., Pinar, M., Xiang, X. and Peñalva, M. A. (2014). Maturation of late Golgi cisternae into RabE^{RAB11} exocytic post-Golgi carriers visualized *in vivo*. *Mol. Biol. Cell* **25**, 2428-2443. doi:10.1091/mbc.e14-02-0710

Peñalva, M. A. (2005). Tracing the endocytic pathway of *Aspergillus nidulans* with FM4-64. *Fungal Genet. Biol.* **42**, 963-975. doi:10.1016/j.fgb.2005.09.004

Peñalva, M. A., Galindo, A., Abenza, J. F., Pinar, M., Calcagno-Pizarelli, A. M., Arst, H. N., Jr. and Pantazopoulou, A. (2012). Searching for gold beyond mitosis: mining intracellular membrane traffic in *Aspergillus nidulans*. *Cell Logist.* **2**, 2-14. doi:10.4161/cl.19304

Peñalva, M. A., Zhang, J., Xiang, X. and Pantazopoulou, A. (2017). Transport of fungal RAB11 secretory vesicles involves myosin-5, dynein/dynactin/p25, and kinesin-1 and is independent of kinesin-3. *Mol. Biol. Cell* **28**, 947-961. doi:10.1091/mbc.e16-08-0566

Pinar, M. and Peñalva, M. A. (2017). *Aspergillus nidulans* BapH is a RAB11 effector that connects membranes in the Spitzenkörper with basal autophagy. *Mol. Microbiol.* **106**, 452-468. doi:10.1111/mmi.13777

Pinar, M., Pantazopoulou, A., Arst, H. N., Jr. and Peñalva, M. A. (2013a). Acute inactivation of the *Aspergillus nidulans* Golgi membrane fusion machinery: correlation of apical extension arrest and tip swelling with cisternal disorganization. *Mol. Microbiol.* **89**, 228-248. doi:10.1111/mmi.12280

Pinar, M., Pantazopoulou, A. and Peñalva, M. A. (2013b). Live-cell imaging of *Aspergillus nidulans* autophagy: RAB1 dependence, Golgi independence and ER involvement. *Autophagy* **9**, 1024-1043. doi:10.4161/auto.24483

Pinar, M., Arst, H. N., Jr., Pantazopoulou, A., Tagua, V. G., de los Ríos, V., Rodríguez-Salarichs, J., Díaz, J. F. and Peñalva, M. A. (2015). TRAPPII regulates exocytic Golgi exit by mediating nucleotide exchange on the Ypt31 ortholog RabE/RAB11. *Proc. Natl. Acad. Sci. USA* **112**, 4346-4351. doi:10.1073/pnas.1419168112

Pinar, M., Arias-Palomo, E., de los Ríos, V., Arst, H. N., Jr. and Peñalva, M. A. (2019). Characterization of *Aspergillus nidulans* TRAPPs uncovers unprecedented similarities between fungi and metazoans and reveals the modular assembly of TRAPPII. *PLoS Genet.* **15**, e1008557. doi:10.1371/journal.pgen.1008557

Riedel, F., Galindo, A., Muschalik, N. and Munro, S. (2017). The two TRAPP complexes of metazoans have distinct roles and act on different Rab GTPases. *J. Cell Biol.* **217**, 601-617. doi:10.1083/jcb.201705068

Rivera-Molina, F. E. and Novick, P. J. (2009). A Rab GAP cascade defines the boundary between two Rab GTPases on the secretory pathway. *Proc. Natl. Acad. Sci. USA* **106**, 14408-14413. doi:10.1073/pnas.0906536106

Sacher, M., Shahrzad, N., Kamel, H. and Milev, M. P. (2018). TRAPPopathies: an emerging set of disorders linked to variations in the genes encoding transport protein particle (TRAPP)-associated proteins. *Traffic* **20**, 5-26. doi:10.1111/tra.12615

Taheri-Talesh, N., Xiong, Y. and Oakley, B. R. (2012). The Functions of Myosin II and Myosin V homologs in tip growth and septation in *Aspergillus nidulans*. *PLoS ONE* **7**, e31218. doi:10.1371/journal.pone.0031218

Takeshita, N., Evangelinos, M., Zhou, L., Serizawa, T., Somera-Fajardo, R. A., Lu, L., Takaya, N., Nienhaus, G. U. and Fischer, R. (2017). Pulses of Ca^{2+} coordinate actin assembly and exocytosis for stepwise cell extension. *Proc. Natl. Acad. Sci. USA* **114**, 5701-5706. doi:10.1073/pnas.1700204114

Thomas, L. L. and Fromme, J. C. (2016). GTPase cross talk regulates TRAPPII activation of Rab11 homologues during vesicle biogenesis. *J. Cell Biol.* **215**, 499-513. doi:10.1083/jcb.201608123

Thomas, L. L., Joiner, A. M. N. and Fromme, J. C. (2018). The TRAPPIII complex activates the GTPase Ypt1 (Rab1) in the secretory pathway. *J. Cell Biol.* **217**, 283-298. doi:10.1083/jcb.201705214

Thomas, L. L., van der Vegt, S. A. and Fromme, J. C. (2019). A steric gating mechanism dictates the substrate specificity of a Rab-GEF. *Dev. Cell* **48**, 100-114.e9. doi:10.1016/j.devcel.2018.11.013

Todd, R. B., Davis, M. A. and Hynes, M. J. (2007). Genetic manipulation of Aspergillus nidulans: meiotic progeny for genetic analysis and strain construction. *Nat. Protoc.* **2**, 811-821. doi:10.1038/nprot.2007.112

Yip, C. K., Berscheminski, J. and Walz, T. (2010). Molecular architecture of the TRAPPII complex and implications for vesicle tethering. *Nat. Struc. Mol. Biol.* **17**, 1298-1304. doi:10.1038/nsmb.1914

Zhang, J., Tan, K., Wu, X., Chen, G., Sun, J., Reck-Peterson, S. L., Hammer, J. A., III and Xiang, X. (2011). *Aspergillus* Myosin-v supports polarized growth in the absence of microtubule-based transport. *PLoS ONE* **6**, e28575. doi:10.1371/journal.pone.0028575

Zhang, J., Qiu, R., Arst, H. N., Jr., Peñalva, M. A. and Xiang, X. (2014). HookA is a novel dynein-early endosome linker critical for cargo movement in vivo. *J. Cell Biol.* **204**, 1009-1026. doi:10.1083/jcb.201308009

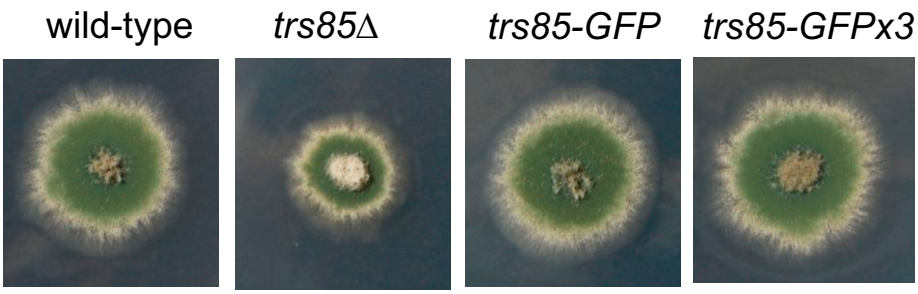

Figure S1. GFP-tagging of Trs85 does not impair growth.
Colonies of the indicated genotypes were cultured on synthetic complete medium for 3 days at 37ºC

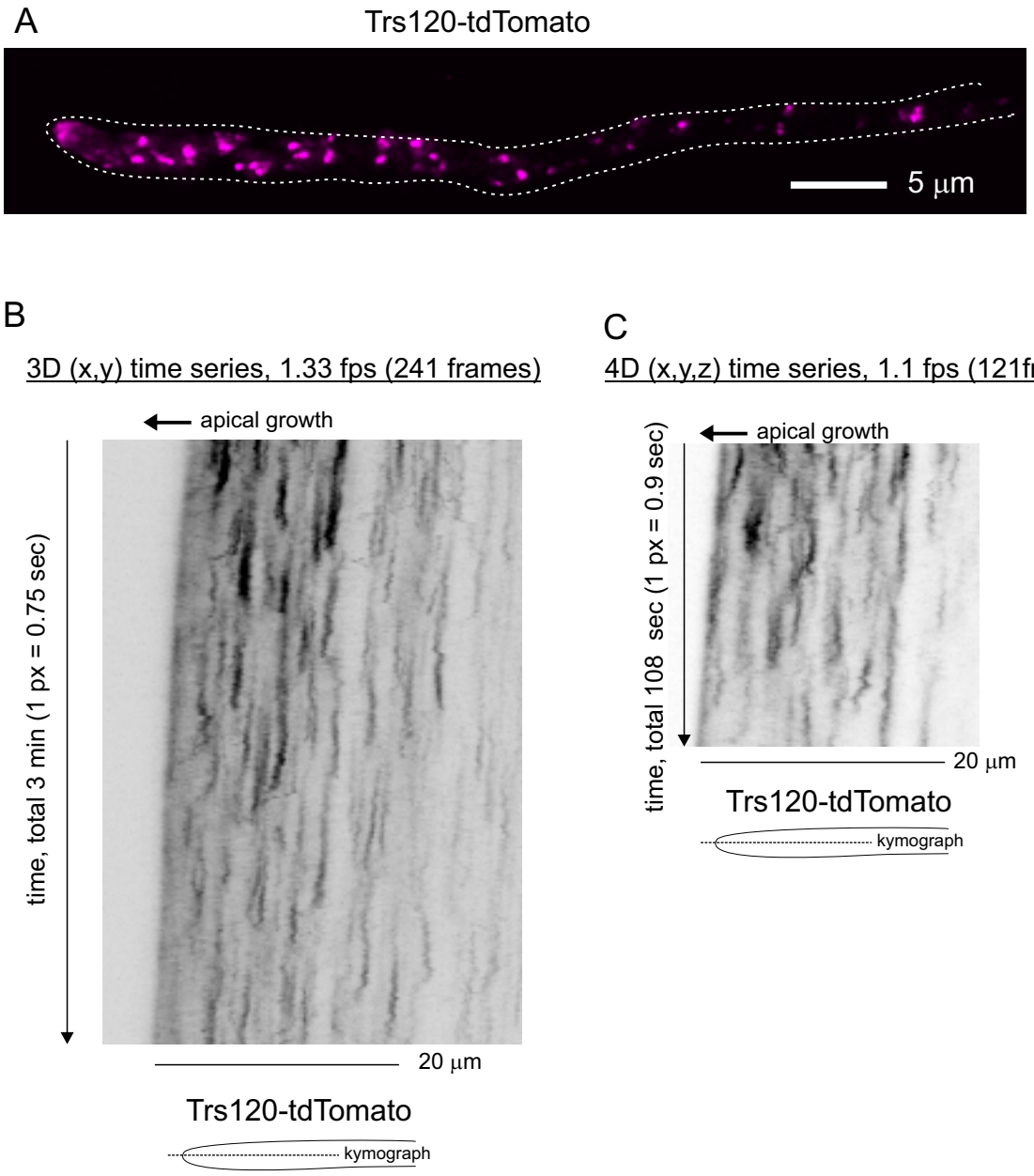

Figure S2. Transient recruitment of TRAPPII to TGN cisternae as determined with Trs120-tdT

(A) Maximal intensity projection of a deconvolved Z-stack of a cell expressing Trs120-tdT. (B)(C) Kymographs derived from 3D and 4D movies illustrating that Trs120-tdT behaves as Trs120-GFPX3 over time. The 3D movie in (B) is 3 min- and 241 frames-long and was acquired with 2x2 binning.

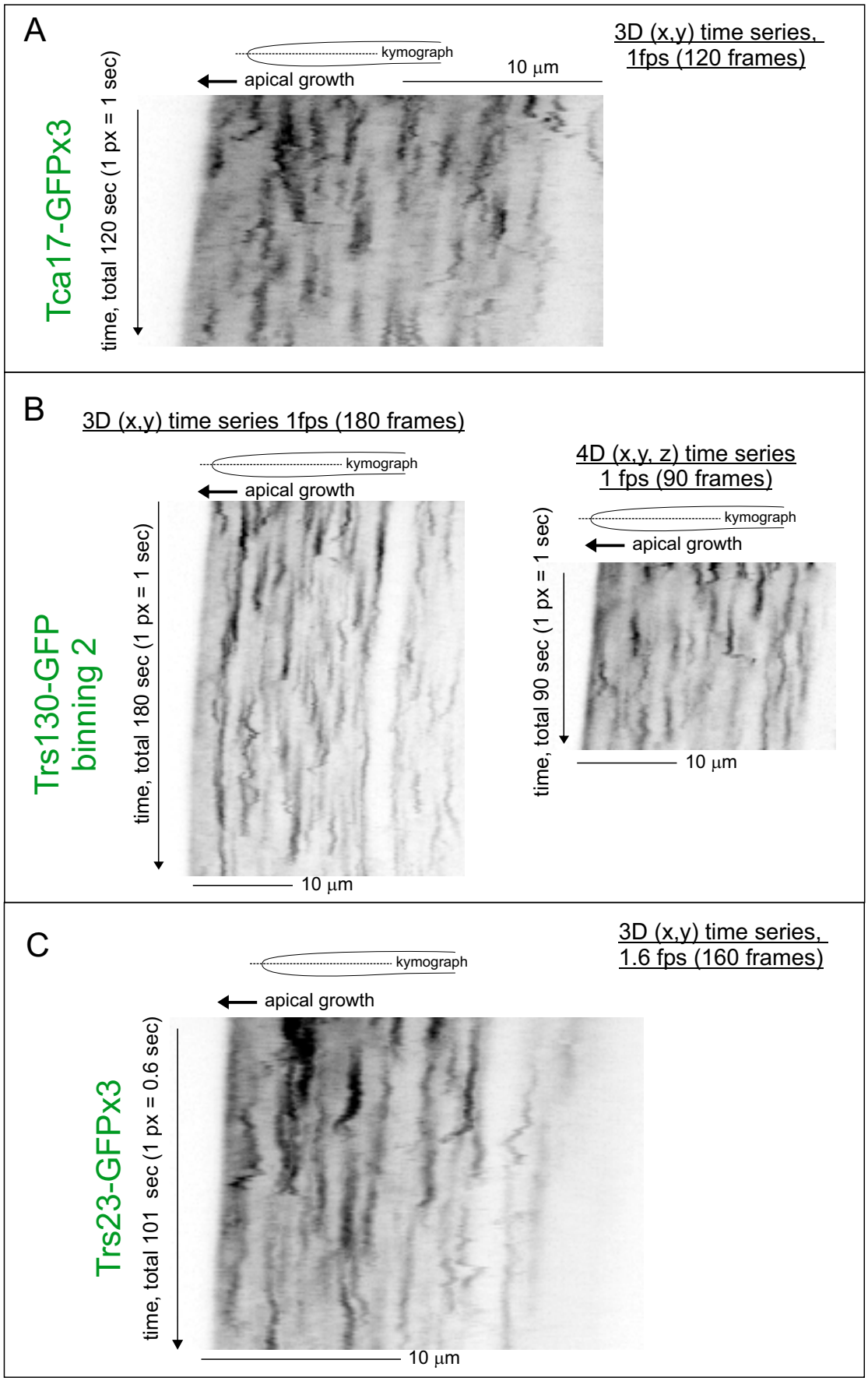

Figure S3. Transient recruitment of other TRAPP subunits to TGN cisternae
3D or 4D movies, as indicated, of strains expressing: (A) Tca17-GFPx3. (B) Trs130-GFP. (C) Trs23-GFPx3. Acquired with the specified conditions.

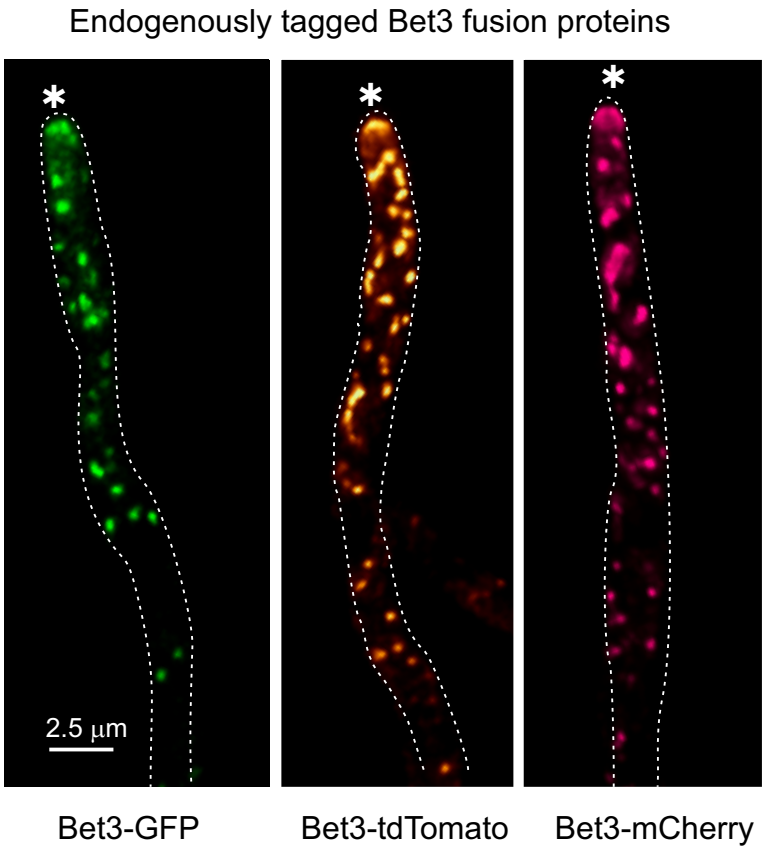

Figure S4. Bet3 localization with different fluorescent protein tags
Images are maximal intensity projections of deconvolved Z-stacks. Asterisks indicate the SPKs

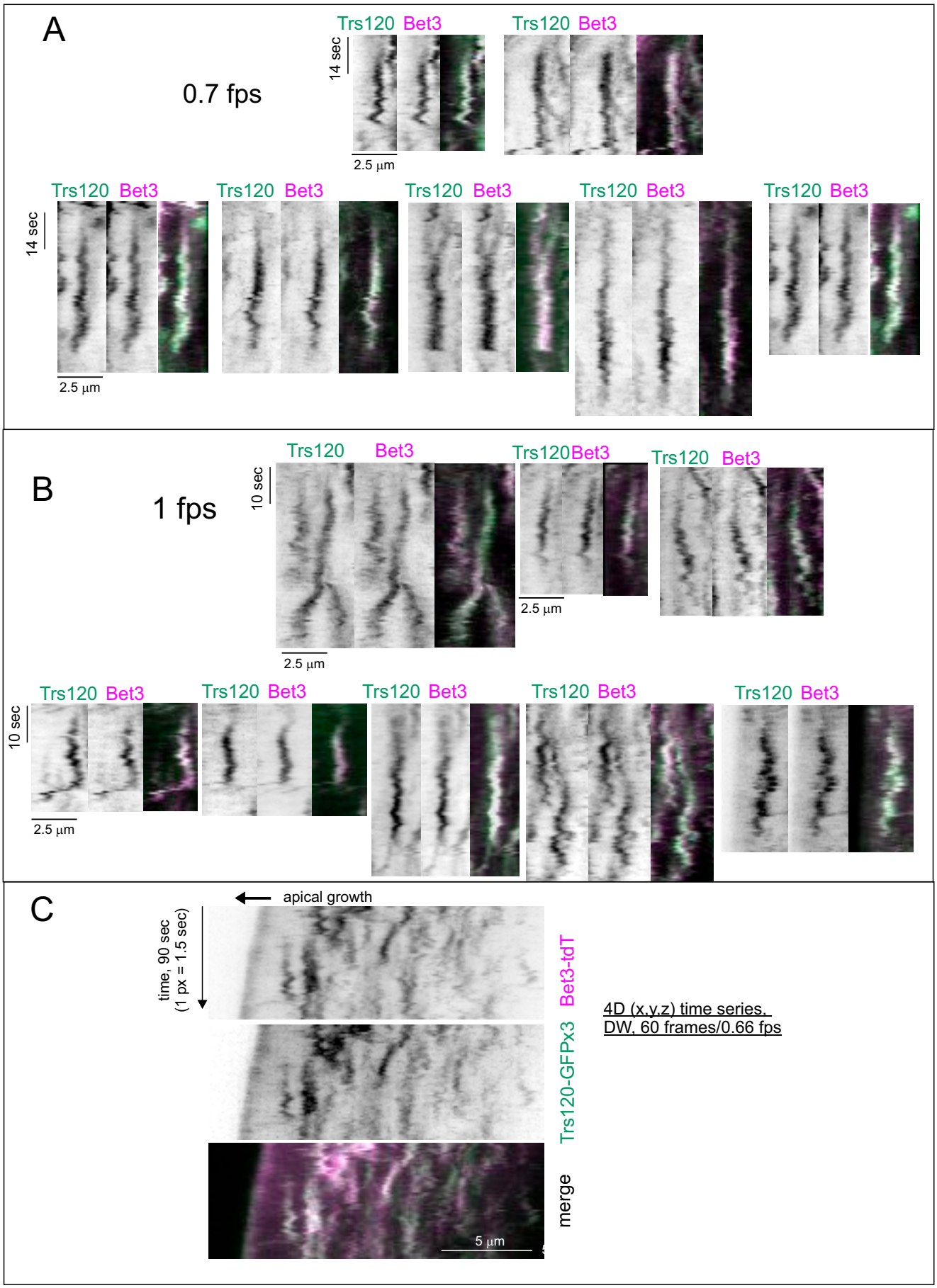

Figure S5. Trs120 and Bet3 strictly colocalize continuously on TGN cisternae. (A) Multiple examples showing that Trs120-GFPx3 and Bet3-tdT simultaneously accumulate at, and dissipate from maturing TGN cisternae. Kymographs from which these examples were extracted were obtained from 3D movies of the two channels simultaneously acquired with a beam splitter at a *Tr* of 0.7 fps. (B) As above, but using 3D movies with a *Tr* of 1 fps. (C) Overall view of a kymograph obtained from a 4D movie acquired with a beam splitter at a *Tr* of 0.66 fps. Note the clear example of the maturing cisterna closest to the SPK.

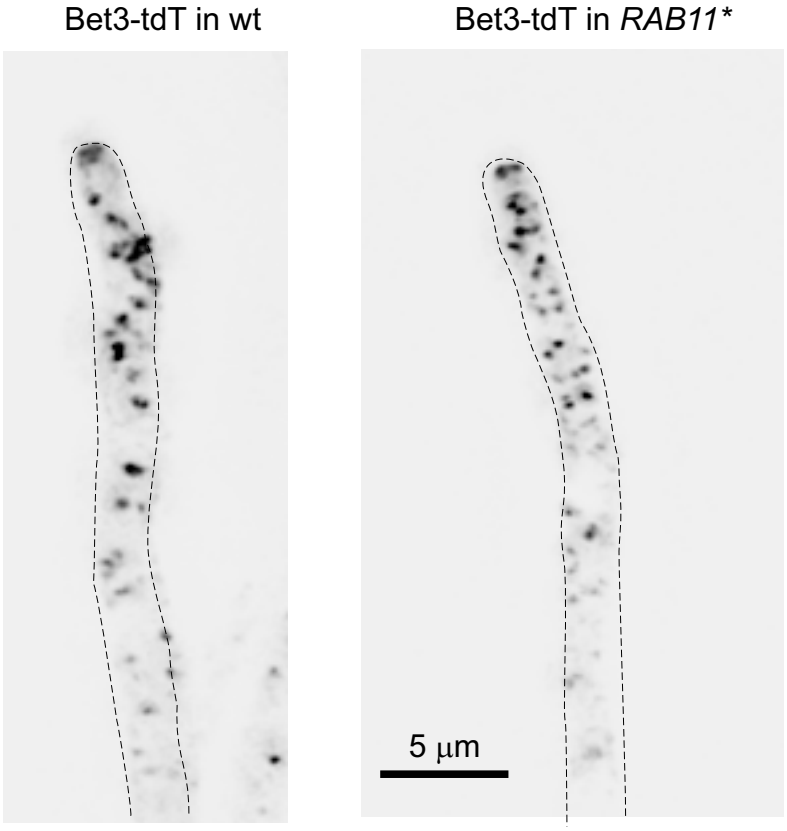

Figure S6. Bet3-tdT localization to the TGN is not altered by RAB11*.
Images are maximal intensity projections of deconvolved z-stacks.

Table S1: Strains used in this work

Strain code	Genotipe
MAD3921	*trs120*::*gfp*::*pyrG*^{Af} *pyrG*89; *pyroA*4 *nkuA*Δ::*bar*
MAD4397	*pyrG*89; *trs85*::*gfp*::*pyrG*^{Af} *pyroA*4 *nkuA*Δ::*bar*
MAD5319	*pyrG*89; *pyroA*4 *nkuA*Δ::*bar*; *riboB*2
MAD5321	*pyroA*4 *nkuA*Δ::*bar*; *riboB*2
MAD5736	*pyrG*89; *pyroA*4 *nkuA*Δ::*bar*
MAD5743	*pyrG*89 *sec7*::*gfp*::*pyrG*^{Af,} *pyroA*4 *nkuA*Δ::*bar*
MAD6305	*pyrG*89; *pyroA*4 *nkuA*Δ::*bar*; *bet5*::*gfp*::*pyrG*^{Af}
MAD6317	*pyrG*89; *bet5*::*mcherry*::*pyrG*^{Af,} *pyroA*4 *nkuA*Δ::*bar*
MAD6381	*pyrG*89; *pyroA*4 *nkuA*Δ::*bar*; *bet3*::*gfp*::*pyrG*^{Af}
MAD6420	*trs20*::*gfp*::*pyrG*^{Af} *pyrG*89; *pyroA*4 *nkuA*Δ::*bar*
MAD6439	*pyrG*89; *trs23*::*gfp*::*pyrG*^{Af} *pyroA*4 *nkuA*Δ::*bar*
MAD6443	*trs31*::*gfp*::*pyrG*^{Af} *pyrG*89; *pyroA*4 *nkuA*Δ::*bar*
MAD6461	*pyrG*89?; *trs85*Δ::*pyrG*^{Af} *nku*Δ::*bar*?; *riboB*2
MAD6610	*trs33*::*gfp*::*pyrG*^{Af} *pyrG*89 *pabaA*1; *nkuA*Δ::*bar*
MAD6635	[*rab11*^{p}::*rabE*::*rab11*^{p}::*mcherry*::*rab11*::*pyrG*^{Af}] *pyrG*89 *pabaA*1; *nkuA*Δ::*bar*
MAD6639	*pyrG*89 *pabaA*1; *nkuA*Δ::*bar*; *bet5*-3x-*gfp*::*pyrG*^{Af}
MAD6648	*trs31*::3x-*gfp*::*pyrG*^{Af} *pabaA*1 *pyrG*89; *nkuA*Δ::*bar*
MAD6672	*trs120*::3x-*gfp*::*pyrG*^{Af} *pyrG*89; *pyroA*4 *nkuA*Δ::*bar*
MAD6726	*pabaA*1 *pyrG*89; *trs23*::3x-*gfp*::*pyrG*^{Af} *nkuA*Δ::*bar*
MAD6760	*trs120*::3x-*gfp*::*pyrG*^{Af} *pyrG*89; *nkuA*Δ::*bar*; [*rab11*^{p}::*rab11*::*rab11*^{p}::*mcherry*::*rab11*::*pyrG*^{Af}]
MAD6780	*pabaA*1 *pyrG*89; *tca17*::*gfp*::*pyrg*^{Af}; *nkuA*Δ::*bar*
MAD6783	*pabaA*1 *pyrG*89; *nkuA*Δ::*bar*; *bet3*::*mcherry*::*pyrG*^{Af}
MAD6807	*trs120*::*tdTomato*::*pyrG*^{Af} *pabaA*1 *pyrG*89; *nkuA*Δ::*bar*
MAD6826	*pabaA*1 *pyrG*89; *nkuA*Δ::*bar*; *bet3*::*tdTomato*::*pyrG*^{Af}
MAD6835	*pyrG*89; *pyroA*4 *nkuA*Δ::*bar*; *trs65*::*gfp*::*pyrg*^{Af}
MAD6837	*pyrG*89; *pyroA*4 *nkuA*Δ::*bar*; *trs130*::*gfp*::*pyrg*^{Af}
MAD6865	*pyrG*89; *tca17*::3x-*gfp*::*pyrg*^{Af}; *pyroA*4 *nkuA*Δ::*bar*
MAD6867	*trs120*::3x-*gfp*::*pyrG*^{Af} *pyrG*89; *pyroA*4 *nkuA*Δ::*bar*; *bet3*::*tdTomato*::*pyrG*^{Af}
MAD6971	*trs120*Δ::*pyrG*^{Af} *pyrG*89; *pyroA*4 *nkuA*Δ::*bar*; bet3::*tdTomato*::*pyrG*^{Af}; *rab11*^{D125E}
MAD6973	*trs120*Δ::*pyrG*^{Af} *pyrG*89; *trs23*::3x-*gfp*::*pyrG*^{Af} *pyroA*4 *nkuA*Δ::*bar*; *rab11*^{D125E}
MAD6982	*sec7*::*gfp*::*pyrG*^{Af} *pyrG*89; *pyroA*4 *nkuA*Δ::*bar*; *bet3*::*tdTomato*::*pyrG*^{Af}
MAD7025	*pyrG*89?; *pyroA*4::[*pyroA**- *gpda*^{mini}::*gfp*::*sedV*] *nkuA*Δ::*bar*?; *pantoB*100; *bet3*::*tdTomato*::*pyrG*^{Af}
MAD7027	*trs120*::*tdTomato*::*pyrG*^{Af} *sec7*::*gfp*::*pyrG*^{Af} *pabaA*1 *pyrG*89; *pyroA*4 *nkuA*Δ::*bar*
MAD7042	*sec7*::*tdTomato*::*pyrG*^{Af} *pyrG*89; *pyroA*4 *nkuA*Δ::*bar*
MAD7044	*pyrG*89; *trs85*::*mcherry*::*pyrG*^{Af} *pyroA*4 *nkuA*Δ::*bar*
MAD7056	*trs120*::3x-*gfp*::*pyrG*^{Af} *sec7*::*tdTomato*::*pyrG*^{Af} *pabaA*1 *pyrG*89; *pyroA*4 *nkuA*Δ::bar
MAD7067	*pabaA*1 *pyrG*89; *trs85*::3x-*gfp*::*pyrG*^{Af} *nkuA*Δ::*bar*
MAD7405	*pyrG*89 *trs120*Δ::*pyrG*^{Af}; *trs85*::3x-*gfp*::*pyrG*^{Af} *pyroA*4 *nkuA*Δ::*bar*; *rab11*^{D125E}
MAD7416	*pyrG*89; *nkuA*Δ::*bar*; *bet3*::*tdTomato*::*pyrG*^{Af}; *rab11*^{D125E}

Supplemental movies

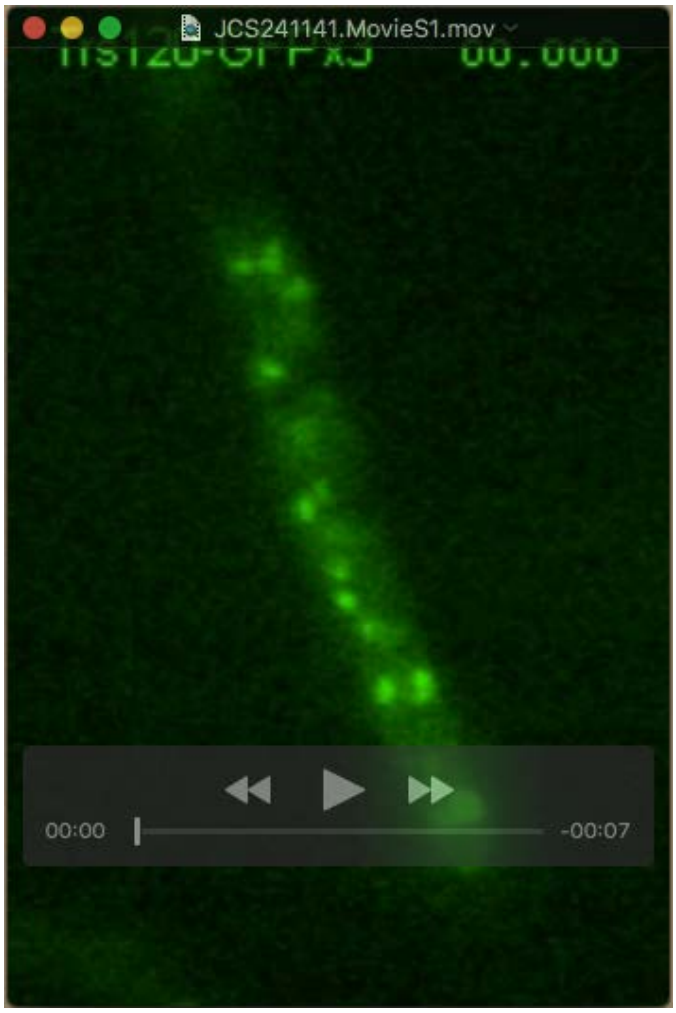

Movie 1: 3D movie of Trs120-GFPx3

Consisting of 210 middle planes acquired every 0.5 sec and reproduced at 30 fps. Time stamp in sec.msec.

Movie 2: 4D movie of Trs120-GFPx3.

Consisting of 120 frames; each frame is the maximal intensity projection of a 2 µm-deep Z-stack acquired every 1.5 sec and reproduced at 30 fps. Time stamp in sec.msec.

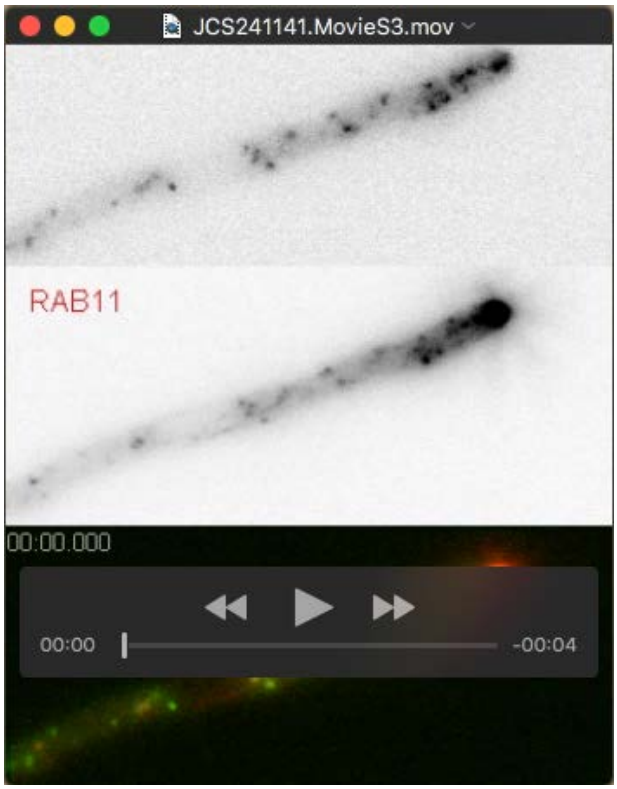

Movie 3: 4D movie of Trs120-GFPx3 and mCh-RAB11

Consisting of 62 frames; each frame is a maximal intensity projection of a Z-stack in which the two channels were simultaneously acquired with a beam splitter every 1.2 sec; the movie is reproduced at 15 fps. Time stamp in min:sec.msec.

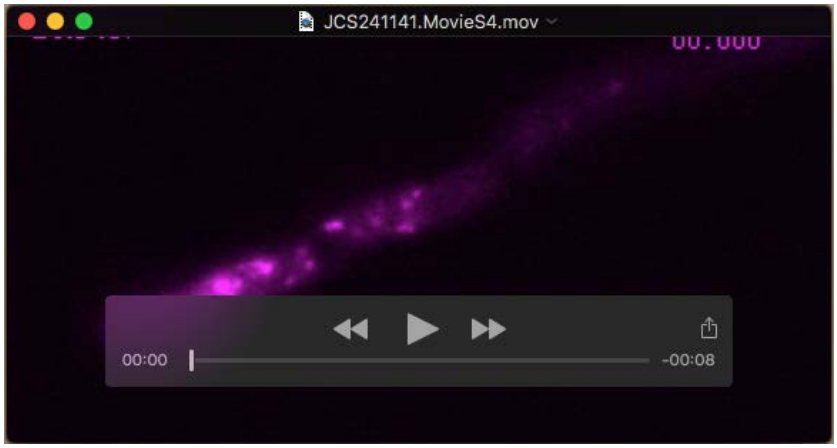

Movie 4: 4D movie of Bet3-tdTomato

Consisting of 120 frames; each frame is a maximal intensity projection of a Z-stack acquired every 1 sec. Reproduced at 15 fps. Time stamp in sec.msec.

Movie 5: 3D movie of Trs120-GFPx3 and Bet3-tdTomato

Consisting of 180 middle planes in which the two channels were simultaneously acquired with a beam splitter every 1 sec; the movie is reproduced at 30 fps. Time stamp in sec.msec.

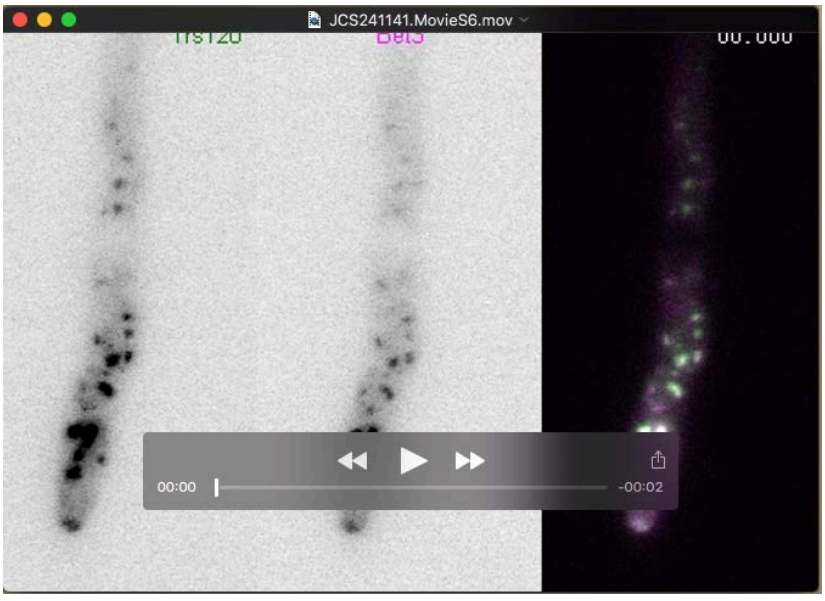

Movie 6: 4D movie of Trs120-GFPx3 and Bet3-tdTomato

Consisting of 61 frames; each frame is a maximal intensity projection of a Z-stack. The GFP and tdT channels were simultaneously acquired every 1.5 sec. Reproduced at 30 fps. Time stamp in sec.msec.